SYSTEMATIC TUNING OF SILICON SCHOTTKY BARRIER HEIGHT BY ATOMIC INTERLAYERS WITH LOW ELECTRONEGATIVITIES

by

WEI LONG

A dissertation submitted to the Graduate Faculty in Physics in partial fulfillment of the requirements for the degree of Doctor of Philosophy, The City University of New York

2012

This manuscript has been read and accepted for the
Graduate Faculty in Physics in satisfaction of the
dissertation requirement for the degree of Doctor of Philosophy.

Prof. Raymond T. Tung

Date | Chair of Examining Committee

Prof. Igor L. Kuskovsky

Date | Executive Officer

Prof. Gregory S. Boutis

Prof. Zhiheng Liu

Prof. Mim Lal Nakarmi

Prof. Aidong Shen

Supervisory Committee

THE CITY UNIVERSITY OF NEW YORK

ABSTRACT

SYSTEMATIC TUNING OF SILICON SCHOTTKY BARRIER HEIGHT BY ATOMIC INTERLAYERS WITH LOW ELECTRONEGATIVITIES

by

Wei Long

Advisor: Professor Raymond T. Tung

The Schottky barrier height (SBH) is of great importance to the functionality of semiconductor devices, as it governs the carrier transport across the metal-semiconductor (MS) interface. The presence of the Fermi level (FL) pinning phenomena makes tuning the SBH a difficult goal to achieve. The technique of "partisan interlayer" (PI) was proposed recently to modify the SBH, where stable adsorbate-terminated semiconductor (ATS) surfaces were used to form SBs with subsequently applied metal. When elements with large electronegativities were used to form the ATS, the PI technique was effective in reducing the n-type SBH and increasing the p-type SBH, driven by the expected transfer of charge from the semiconductor to the adsorbates. In this thesis work, elements with electronegativities smaller than that of the semiconductor are used as surface termination. SBHs for Ag, Au and In on Si surfaces are found to increase for the n-type and decrease for the p-type interfaces, by as much as 0.25eV, when Ga, Mg and K are used to terminate the Si surfaces. The present results are thus in agreement with the expected charge transfers from elements with smaller electronegativities to silicon and illustrate the general validity of the PI technique. The chemical stability of these surfaces likely weakens the MS interaction and leads to the (partial) preservation of the surface dipole at the MS interface. However, large degrees of SBH inhomogeneity are observed for diodes on these surfaces, likely

due to insufficient stability of these surfaces to completely withstand metal interaction. These results are discussed within the basic models of SBH formation and the implications of these results for SBH control of MS systems are also addressed.

ACKNOWLEDGEMENT

The writing of this dissertation, having been a momentous academic challenge I have ever faced, could never have been achieved without the generous guidance, support, help and patience from my advisor, thesis committee members, faculty and staff at the Brooklyn College of CUNY, fellow students, friends and all family members. It is to them that I own my deepest gratitude.

I have been fortunate to have my advisor, Prof. Raymond Tung, the gentleman always pursuing the ultimate truth with his wisdom, knowledge and commitment to the highest standard. I wish to thank him again for the excellent supervision and tremendous inspiration surrounded in such a scientific atmosphere that I can benefit greatly. I am also grateful to all my thesis committee members for their munificent comments and for their courtesy that made the defense possible in the summer of 2012.

I am indebted to many faculty and staff at the Brooklyn College to support my research work, especially to Prof. Zhiheng Liu, who magnanimously granted our access to his apparatus which have made a significant contribution to my research, and to machine shop technicians Louis Tundis and Zakhar Yudovin, who eventually brought our UHV system into a reality.

I could have been more than lonely without all my fellow students and friends, especially Yang Li. I wish, but have never got an opportunity, to thank Samil E. Ogun, to whom this thesis is dedicated, a senior PhD candidate who passed away in 2008, for being such a nice guy and a good friend of mine. His name, with his beloved team, Galatasaray, will always be remembered.

Finally, I thank my parents and my girl friend Yolanda Zhu, who were cheering me up, encouraging me and supporting me through all good times, and bad.

TABLE OF CONTENTS

LIST OF TABLES

LIST OF FIGURES

CHAPTER 1. Background

As modern electronic and optoelectronic devices often integrate/assemble dissimilar materials with different functionalities together on a nanometer scale, the control of the electrical integrity of the conglomerate becomes a formidable issue and is of paramount importance to the overall performance of the devices. Carrier transport in these structures is affected by the band alignment condition at many of the interfaces either directly in line of, or peripheral to, the conduction path. The ability to control the band offset at solid interfaces, which is obviously a desirable and even necessary skill to master for these applications, however remains a capability we presently do not own. At metal-semiconductor (MS) interfaces, which constitute one of the most important classes of technological interface, the control of the band-offset, which is also known as the Schottky barrier height (SBH), has been difficult due to the well-known Fermi-level (FL) pinning phenomenon. Presently, the formation mechanism of the SBH still remains a subject of much debate [1, 2]. In the literature, there have been sporadic demonstrations that the magnitude of SBH can be moderately adjusted by altering the atomic structure of the MS interface, applicability of such a strategy is limited to very few (epitaxial) MS systems [3, 4]. Empirical methods such as low deposition temperature [5], thin insulator layer [6, 7] and surface passivation with chalcogen [8, 9] have shown an ability to change the SBH to some extent, but none has developed into a viable and practical technology. In this chapter, existing models for the formation of the SBH [1, 4, 10, 11] are briefly discussed.

1.1. Schottky Barrier

The Schottky barrier (SB), as one of the most interesting properties of the metal-semiconductor systems, governs the electronic transport across the MS interfaces, and therefore, is of vital importance to the successful operation of virtually all the semiconductor devices. When a metal and a semiconductor are brought into intimate contact with thermal equilibrium established, the SBH measures the energy difference between metal Fermi level and the majority band edge of the semiconductor [12]. The first order theory of the barrier height was the original Schottky-Mott model [13, 14], based on the assumption that the charge distributions on the free surfaces of the isolated metal and semiconductor crystals remain frozen upon the formation of the MS interface. Within this non-interacting Schottky-Mott theory, the spatial gap between the metal and the semiconductor is envisioned to be reduced to zero, while the relative position of the bands of the semiconductor and the metal remains unchanged (See Fig. 1) according to the superposition principle of electrostatic potential. The resultant SBH $\Phi_{B,n}^{0}$ to n-type semiconductor is given by

$$\Phi_{B,n}^{0} = \phi_M - \chi_S , \tag{1}$$

where ϕ_M is the work function (WF) of the metal, and χ_S is the semiconductor electron affinity (EA). Conversely, an idealistic SBH between metal and p-type semiconductor is

$$\Phi_{B,p}^{0} = E_g - \left(\phi_M - \chi_S\right). \tag{2}$$

Because of its sound basis in the superposition principle, the Schottky-Mott model is valid whenever the rearrangement of charge during the formation of the MS interface can be ignored [10, 11]. Since significant charge redistributions at a MS interface usually occur when new bonds

are formed and/or old bonds are broken, the Schottky-Mott model is not expected to give accurate predictions of SBH at common MS interfaces where interface bonding is unavoidable. In practice, the Schottky-Mott model failed to explain the absence of strong dependence of the magnitude of SBH on metal WF.

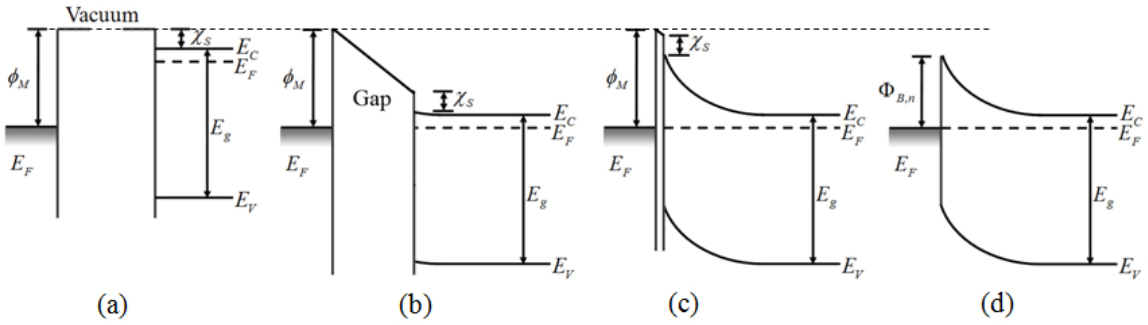

Figure 1. Schematic energy-band diagrams of MS contacts. Metal and semiconductor (a) in isolated systems, and (b) connected into one system. As the gap (c) is reduced and (d) approaches zero, a SB is formed. (After Ref. 12)

1.2. Fermi Level Pinning Phenomenon

The strong dependence of the SBH on the metal WF of the Schottky-Mott model can also be expressed as

$$S_\Phi \equiv \frac{\partial \Phi_{B,n}^0}{\partial \phi_M} = 1, \tag{3}$$

where S_Φ is known as the interface behavior parameter, or the S-parameter, of the semiconductor. The SBHs measured in actual experiments often showed some dependence on the preparation of the MS interface, which indicates that the SBH depends on more than just the WF of the metal. Despite some scatters in the experimental data, by and large, metals with larger

WF's have been found to have systematically higher SBHs than those with lower WF's. However, the actual dependence is much weaker than that predicted by Schottky-Mott model and the S-parameter is usually found to be much smaller than unity [15]. A term, "Fermi-level (FL) pinning" [16], has been commonly used to describe the insensitivity of the experimental SBH to the metal WF. The failure of the non-interacting Schottky-Mott model to account for experimentally observed SBH is well understood to arise from its neglect of MS interaction and the resultant, additional, interface dipole. Traditionally, the additional dipole has been modeled rigidly as the result of charge exchange between the metal and the surface/interface states residing on the semiconductor, over a fixed distance assumed to be the interface distance. In a simplified view adopted by many models, the surface/interface states are further assumed to be entirely a property of the semiconductor, leading to semi-quantitative explanation of experimentally observed FL pinning behavior [17-23]. However, the common assumption of the independence of the interface states on the metal, which underpins many "interface state models", does not agree with experimental results [3, 4] and has also been repeatedly dismissed by *ab initio* calculations [24-26]. An alternative view on the formation of the interface dipole, cast without specific reference to interface states, focused on chemical bond formation at MS interfaces and showed that the expected bond polarization alone could account for the experimentally observed interface dipoles [10, 11], which will be discussed separately in the following chapter.

1.3. Current Transport Properties - Thermionic Emission Theory

The carrier transport though a MS interface, for a SBH under forward bias with lightly doped semiconductor operated at moderate temperatures, is expected to be conducted overwhelmingly by the majority carriers [12, 27]. Several models, e.g. thermionic-emission

theory by H. Bethe [28], diffusion theory by W. Schottky[14] and thermionic-emission- diffusion theory by C. Crowell and S. Sze [29], based on different assumptions of the dominant processes in the interface region, were proposed. The thermionic emission process was found to dominate the carrier transport [30, 31] and the thermionic emission theory was found adequate to describe transport properties for common high-mobility semiconductors, e.g., Si and GaAs.

The thermionic emission theory [27, 28] states that the thermionic emission of carriers over a neighboring energy barrier with maximum height Φ above the (quasi) FL is given by

$$I_{uni-directional} = A^* A T^2 \exp\left(\frac{-\Phi}{k_B T}\right), \tag{4}$$

where A is the cross-sectional area of the barrier, A^* is the Richardson's constant, k_B is the Boltzmann constant and T is absolute temperature. More specifically, for a uniform SB with height Φ_B^0 under an applied bias V_a, the current flowing from n-type semiconductor to metal (defined as forward direction in this case) can be written as

$$I_{forward} = A^* A T^2 \exp\left(\frac{-\Phi_B^0 + eV_a}{k_B T}\right), \tag{5}$$

with the reverse current (flowing from metal to n-type semiconductor by definition), which is also known as saturation current I_S that is independent of V_a, given by

$$I_{reverse} = I_S = A^* A T^2 \exp\left(\frac{-\Phi_B^0}{k_B T}\right). \tag{6}$$

Total (forward) current is therefore

$$I_{total} = A^* A T^2 \exp\left(\frac{-\Phi_B^0}{k_B T}\right)\left[\exp\left(\frac{eV_a}{k_B T}\right)-1\right] = I_S\left[\exp\left(\frac{eV_a}{k_B T}\right)-1\right]. \quad (7)$$

1.4. Measurement of Schottky Barrier Height

Generally, current-voltage (I-V), activation-energy (A-E), capacitance-voltage (C-V) and photoelectric methods (P-E) are commonly used techniques for SBH measurement. In the present work, an extensive study of the temperature-dependent electrical characteristics of SB junctions fabricated on various ATS surfaces was carried out with I-V, C-V and A-E techniques.

1.4.1. Current-Voltage (I-V) Measurement

The carrier transport though a MS interface is given by thermionic emission theory, with the total current density being written as

$$J = A^* T^2 \exp\left(\frac{-\Phi_B}{k_B T}\right)\left[\exp\left(\frac{eV_a}{nk_B T}\right)-1\right], \quad (8)$$

where A^*=112A/cm^2-K^2 for n-type Si and n is the ideality factor. Logarithmic of J is plotted against applied voltage V_a on an I-V graph. By fitting the current density in the forward bias region ($eV_a > 3k_B T$) with the thermionic emission equation, the saturation current density

$$J_0 = A^* T^2 \exp\left(\frac{-\Phi_B}{k_B T}\right), \quad (9)$$

could be obtained by extrapolating the fitted line to y-axis (V_a=0). The magnitude of SBH is related to J_0 as

$$\Phi_B = k_B T \ln\left(\frac{A^* T^2}{J_0}\right). \tag{10}$$

For the idealistic case (uniform interface and homogeneous SB), the ideality factor is expected to be unity. And reverse current density is dominated mainly by Schottky-barrier lowering, or $J_R = J_0$. However, for most practical Schottky diodes, with the existence of a certain degree of inhomogeneity, the ideality factor is inevitably found to be greater than unity and reverse current density does not really saturate at large reverse bias due to significant tunneling current [32, 33] with contributions from areas with low SBH's [34], especially at low temperature.

1.4.2. Activation-Energy (A-E) Measurement

Activation-energy method (or Richardson's A-E plot) is important in studying SBH in case of unknown active contacting area at MS interface that essentially corroborates SBH systematics deduced from individual temperatures. Multiplying thermal emission equation for forward current density by A, the unknown active area, and neglecting the "1" in the bias dependence, one gets the logarithm of the total forward current divided by temperature squared as

$$\ln\left(\frac{I_F}{T^2}\right) = \ln\left(A^* A\right) - \frac{\Phi_B - eV_a}{k_B T}, \tag{11}$$

where $\Phi_B - eV_a$ is the activation energy. For a fixed forward bias V_a, SBH can be calculated from the plot of $\ln\left(I_F/T^2\right)$ versus $1/k_B T$ as

$$\Phi_B = eV_a - \frac{d\left[\ln\left(I_F/T^2\right)\right]}{d\left(1/k_B T\right)}. \tag{12}$$

It should be reasonable and also convenient to let $V_a = 0$, as I_F is simply the saturation current density deduced from I-V plot multiplied by area A. Thus the magnitude of SBH is expected to be equivalent to the (negative) slope of the A-E curve. Information of active conducting area A can be rendered from the intercept at $1/k_BT = 0$. Practically, for a real Schottky diode formed at non-uniform MS interface, A-E measurement is more sensitive to the low SBH areas. Therefore, a lower value of the magnitude of SBH and smaller active conducting area compared to its geometrical dimensions are consistently expected.

1.4.3. Capacitance-Voltage (C-V) Measurement

When a Schottky junction formed at MS interface, bound space charge due to band bending in the depletion-region varies with applied bias, which defines a capacitance of the junction. If a small alternating signal is applied to the SB under a certain bias V_a, the depletion-region capacitance per unit area C is given by

$$\frac{1}{C^2} = \frac{2\left[\phi_{bi} - V_a - (kT/e)\right]}{e\varepsilon_s N_D}, \tag{13}$$

where ϕ_{bi} is build-in voltage of the diode, ε_s is the dielectric constant of the semiconductor and N_D is the doping concentration in the semiconductor. As $1/C^2$ being plotted against V_a, ϕ_{bi} should be indicated by the intercept on voltage axis. For n-type SB, the magnitude of SBH is given by

$$\Phi_{B,n} = e\phi_{bi} + e\phi_n + k_BT, \tag{14}$$

with ϕ_n being difference between Fermi level and conduction band minimum (CBM) of the semiconductor. For Si,

$$\phi_n = \frac{k_B T}{e} \ln\left(\frac{N_C}{N_D}\right),\ N_C = 2.8\times10^{19}\text{cm}^{-3}. \tag{15}$$

Similarly, p-type SBH is given by

$$\Phi_{B,p} = e\phi_{bi} + e\phi_p + k_B T, \tag{16}$$

where

$$\phi_p = \frac{k_B T}{e} \ln\left(\frac{N_V}{N_A}\right),\ N_V = 2.65\times10^{19}\text{cm}^{-3}. \tag{17}$$

Besides, the doping concentration N_D can be deduced from the C-V plot by

$$N_D = \frac{2}{e\varepsilon_s}\left[-\frac{1}{d\left(1/C^2\right)/dV}\right]. \tag{18}$$

Generally speaking, the magnitude of SBH by C-V measurement is greater than that calculated from I-V and A-E plots, because C-V is insensitive to the inhomogeneity of the SBH. In most cases, multi-frequency C-V measurements are preferable to eliminate the effect of trapped charge and deep level impurities.

1.4.4. Photoelectric Measurement

Photocurrent can be measured when a monochromatic light is incident on a Schottky diode. The square root of photocurrent per absorbed photon, or photoresponse, is proportional to

the difference between SBH and incident photon energy. If the square root of photoresponse is plotted as a function of photon energy, the extrapolated value on the energy axis indicates the SBH Φ_B. Due to limited measurement techniques, photoelectric measurement was not performed in addition to those electrical characterizations.

1.5. Current Transport - Inhomogeneous Schottky Barrier

Existing transport theories are proposed based on the basic assumption that the SBH is homogeneous. However, it was demonstrated both experimentally [3, 35, 36] and theoretically [24, 37] that for epitaxial MS interfaces, the SBH depends on the structure of the interface, which implied that in a non-epitaxial system the SBH should be inhomogeneous. A general theory was presented by R. Tung on the electron transport at non-degenerate MS interfaces with arbitrary SBH distributions [34, 38].

Traditionally, electron transport at an inhomogeneous interface was described by parallel conduction model [39-41]. The current is assumed to be a sum of currents flowing in individual conducting patches (I_i) independently, each with its own area (A_i) and SBH (Φ_i):

$$I(V_a) = \sum_i I_i = A^* T^2 \left[\exp(\beta V_a) - 1\right] \sum_i A_i \exp\left(-\beta \Phi_i\right), \tag{19}$$

with $\beta \equiv q/k_B T$. However, since no interaction between neighboring patches has been considered, this model is in significant error when the spatial distribution of patches with different SBH's is on a scale less than, or comparable to the depletion region width [42, 43].

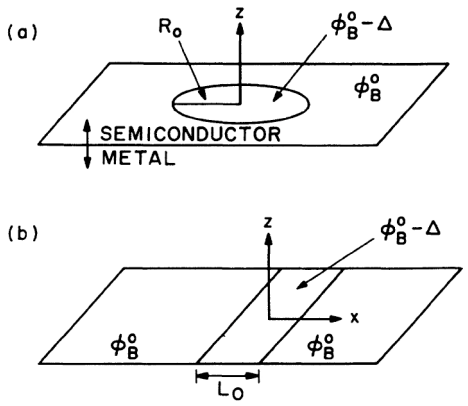

Figure 2. Geometries and coordinates of examples used in the present work. (a) Circular patch, (b) narrow strip. (After Ref. 34)

Conducting path in front of a small patch with low-SBH is "pinched-off" by the surrounding high potential patches, resulting in a higher effective SBH seen by majority carriers. It has been shown that it is easier for pinch-off to occur, for lower doping level and smaller dimension of low-SBH patch. When potential-pinch off occurs, the potential barrier at MS interface increases with applied bias, which is a significant impact on electron transport properties for inhomogeneous Schottky junctions.

1.5.1. An Isolated Region with a Low SBH

If an isolated region, as shown in Fig. 2, with a local SBH of $\Phi_B^0 - \Delta$ is surrounded by regions with a uniform SBH of Φ_B^0, the net current flowing through the interface can be written as

$$I_{patch} = A^* T^2 \left(\frac{4\pi\eta^{2/3}\gamma_0}{9\beta V_{bb}^{2/3}} \right) \exp\left(-\beta\Phi_B^0 + \frac{\beta\gamma_0 V_{bb}^{1/3}}{\eta^{1/3}} \right) \left[\exp(\beta V_a) - 1 \right]. \tag{20}$$

with parameters being summarized in Table I, where $V_{bb} = \Phi_B^0 - V_n - V_a$ is the band bending, $W = \left(2\varepsilon_S V_{bb}/qN_D\right)^{1/2}$ is depletion region width and $\eta \equiv \varepsilon_S/\left(qN_D\right)$.

Table I. Electron transport at an isolated region with a local SBH of $\Phi_B^0 - \Delta$ surrounded by regions with a uniform SBH of Φ_B^0. (After Ref. 34)

Geometry	Circular patch	Semi-infinite strip
Dimension	Radius $= R_0$	Width $= L_0$, length $= L_{\text{strip}} \gg L_0$
Region parameter	$\gamma = 3(\Delta R_0^2/4)^{1/3}$	$\omega = 2(\sqrt{2}L_0\Delta/\pi)^{1/2}$
Space-charge parameter	$\Gamma = (R_0^2\Delta/2W^2V_{\text{bb}})^{1/3}$	$\Omega = (L_0\Delta/2\pi WV_{\text{bb}})^{1/2}$
Saddle-point position	$(\rho = 0, z = \Gamma W)$	$(0, y, z = \Omega W)$
Effective area	$A_{\text{eff}} = (4\pi\gamma/3\beta)(\eta/V_{\text{bb}})^{2/3}$ $= (4/3)\pi\lambda_D^2\Gamma$	$A_{\text{eff}} = (\pi\omega/\beta)^{1/2}(\eta/V_{\text{bb}})^{3/8}L_{\text{strip}}/2$ $= \sqrt{\pi\Omega}\lambda_D L_{\text{strip}}$
Effective SBH	$\Phi_{\text{eff}} = \Phi_B^0 - 3\Gamma V_{\text{bb}}$ $= \Phi_B^0 - \gamma(V_{\text{bb}}/\eta)^{1/3}$	$\Phi_{\text{eff}} = \Phi_B^0 - 4\Omega V_{\text{bb}}$ $= \Phi_B^0 - \omega(V_{\text{bb}}/\eta)^{1/4}$
Ideality factor	$n \approx 1 + \Gamma$ $= 1 + \gamma\eta^{-1/3}V_{\text{bb}}^{-2/3}/3$	$n \approx 1 + \Omega$ $= 1 + \omega\eta^{-1/4}V_{\text{bb}}^{-3/4}/4$

Compared with the conventional thermionic emission equation, an effective area A_{eff} and an effective SBH Φ_{eff} can be defined. Note that effective SBH increases with applied bias, and it is this bias dependence leading to an ideality factor greater than unity.

1.5.2. SB Diodes Consisting of Many Low-SBH Regions

The current flowing across an inhomogeneous SB consisting of many low-SBH regions can be expressed as the sum of currents going through patches with individual $A_{eff,i}$ and $\Phi_{eff,i}$, which are bias-dependent, as

$$I(V_a) = A^* T^2 \left[\exp\left(\beta V_a\right) - 1\right] \sum_i A_{eff,i} \exp\left(-\beta\Phi_{eff,i}\right). \tag{21}$$

(1) Sharply distribute low-SBH patches and/or strips

The current flowing in a SB with a low density of patches c_1, with almost identical γ_0 may be written as

$$I_{total} = A^* T^2 A \exp\left(-\beta\Phi_B^0\right)\left[\exp\left(\beta V_a\right)-1\right]\times\left[1+\frac{4c_1\pi\eta^{2/3}\gamma_0}{9\beta V_{bb}^{2/3}}\exp\left(\frac{\beta\gamma_0 V_{bb}^{1/3}}{\eta^{1/3}}\right)\right], \tag{22}$$

with two components: the characteristics of a SBH of Φ_B^0, and the current dominated by saddle-point potential $\Phi_B^0 - \gamma_0 V_{bb}^{1/3}\eta^{-1/3}$ of the low-SBH region. When c_1 and/or γ_0 are large, the total current will be governed by the low-SBH patches for all practical bias and temperature ranges.

(2) Broad distribute of SBH variation

For a SB diode with an equal number of low-SBH and higher-than-average SBH patches that gives a overall average SBH of Φ_B^0, by ignoring the contribution from the higher-than-average SBH patches, the total current is given by

$$I_{total} = A^* T^2 A \exp\left(-\beta\Phi_B^0\right)\left[\exp\left(\beta V_a\right)-1\right]\times\left[1+f\left(V_{bb}\right)\exp\left(\beta^2\kappa V_{bb}^{\xi}\right)\right], \tag{23}$$

where parameters are defined in Table II.

The current has a component of that going through the entire diode with a uniform SBH Φ_B^0, with an additional current due to the low-SBH regions with an overall effective SBH of $\Phi_{eff} = \Phi_B^0 - \beta\kappa V_{bb}^{\xi}$. And the I-V curves may have a stronger temperature dependence than that from sharply distributed low-SBH patches, as n is given by $n \approx 1 + \xi\beta\kappa V_{bb}^{\xi-1}$.

Table II. Parameters for electron transport at an inhomogeneous SB with a broad distribution of SBH's. (After Ref. 34)

Parameter	Patch	Strip
ξ	$\frac{2}{3}$	$\frac{1}{2}$
κ	$\frac{\sigma_1^2}{2\eta^{2/3}}$	$\frac{\sigma_2^2}{2\eta^{1/2}}$
$f(\beta, V_{bb})$	$\frac{8c_1\sigma_1^2\pi\eta^{1/3}}{9V_{bb}^{1/3}}$	$\frac{c_2\pi\sigma_2^{3/2}\sqrt{\beta}\eta^{1/8}L_{strip}}{1.46V_{bb}^{1/8}}$

1.5.3 SBH Anomalies

Experimentally, SBH anomalies such as leakages and edge-related currents [44], greater-than-unity ideality factors [38], T_0 anomaly [45-47], soft reverse characteristics [48, 49] and dependence of SBH on measurement technique [50-52] were largely reported. In the present work, above non-ideal behaviors of SBH were also consistently observed, which were, as demonstrated, natural consequences of SBH inhomogeneity at MS interface.

CHAPTER 2. Introduction to Partisan Interlayer Technique

2.1 Interface Dipole

FL pinning has historically been modeled, some inconsistencies notwithstanding, as the result of charge transfer between the metal and states, either surface states [17, 18, 22] or metal induced gap states [19-21], attributable to the semiconductor. However, the general assumption of the independence of the interface states on the metal does not agree with experimental results and has also been repeatedly dismissed by *ab initio* calculations. An alternative explanation of the interface dipole $e\Delta_{MS}$, involving polarized bonds at the MS interface, has been proposed and shown to provide semi-quantitative explanation of the FL pinning effect [10, 11] as

$$\Phi_{B,n}^{0} = \phi_M - \chi_S + e\Delta_{MS}. \tag{24}$$

Within this point of view, the interface dipole depends on, and therefore can be controlled by, the atomic structure of the interface. In the same vein, the strength of FL pinning could, in principle, be reduced if some (meta-stable) atomic structures of the interface can be fabricated without strong bonds across the interface.

2.2 Partisan Interlayer

Any effective method to modify the SBH must have a strategy to overcome or weaken the FL pinning effect. It was with these expectations that a "partisan interlayer" (PI) method was proposed recently to modify the SBH, where stable adsorbate-terminated semiconductor (ATS) surfaces were used to form SB with subsequently applied metal [53]. With the strength of FL pinning expected to be weakened by the chemical stability of the ATS surface structure, the

variation of the EA of the ATS surface with the chemical nature of the adsorbate was envisioned to shift the overall SBH.

In a nutshell, an interfacial atomic layer (interlayer) at an MS interface is a single, atomically-sharp, layer of "foreign" atoms inserted between the semiconductor and the metal. From the perspective of modifying the overall interface dipole, the most relevant property of an interlayer is the electronegativity of its atomic species. Without specific reference to the valence number, crystal structure, or the bond lengths in the interface region, how the overall interface dipole should vary with the electronegativity of the interlayer is not readily predictable from simple chemistry (see Fig. 3). An implicit requirement for applying the concept of electronegativity to a system is thermal equilibrium, i.e. all atoms under discussion belong to the same molecule. As mentioned above, a possible strategy to escape equilibrium chemistry is to create meta-stable structures. When breakage in chemical bonds results in neutral "sub-systems" un-bonded to each other, the total dipole of the entire system becomes dominated by charge-transfers within "sub-systems". As an example, Fig. 3(c) depicts a "partisan interlayer" that is bonded only to the semiconductor, leaving the interlayer-metal (I-M) interface un-bonded or only weakly bonded.

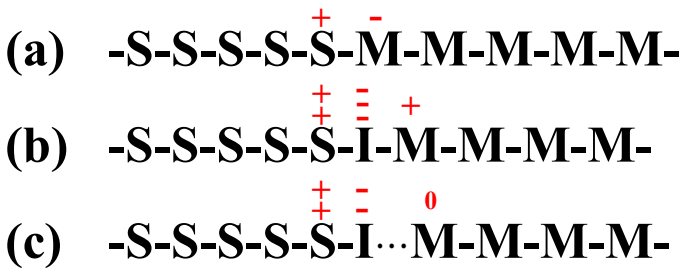

Figure 3. Schematic representations of atomic layers making up metal (M) – interlayer (I) – semiconductor (S) interfaces and the formation of interface dipole.

Interfaces formed as: (a) intimate MS interface; (b) interlayer bonded to both sides; (c) interlayer preferentially bonded to the semiconductor. Horizontal bars indicate bonding between atomic layers. The electronegativites are assumed to be in the order I > M > S. The numbers of signs are meant to roughly indicate the net charge associated with each atomic layer. Note that the interlayer in (b) attracts more electrons from S than M, giving rise to an overall dipole with the same sign as (a). Whether the magnitude of this dipole is larger or smaller than that in (a) depends on details of the chemical bonds. A similar ambiguity exists if the interlayer has a very low electronegativity or one that's intermediate between the metal and the semiconductor.

The lack of strong bonds between the interlayer and the metal (IM) translates to the absence of a large dipole across that interface, i.e. the "pinning" at that interface is weak. As a result, the overall dipole at the (S-I···M) interface is largely dominated by that of interlayer-semiconductor interface (IS) which may be large and adjustable through the choice of the interlayer. The "non-interacting" junction between an I-terminated semiconductor and a metal, depicted in Fig. 3(c), is exactly the type of interface the Schottky-Mott theory is well suited to describe. However, since the "partner" of the metal is the ATS, it is the EA of the latter, χ_{ATS} , that should enter into the Schottky-Mott model as

$$\Phi_{B,n}^{ATS} = \phi_M - \chi_{ATS} + e\Delta_{IM} \approx \phi_M - \chi_{ATS}, \tag{25}$$

where $e\Delta_{MS}$ the dipole due to interactions at the unbonded metal-ATS interface, is expected to be small.

In terms of the ability to induce a large change in the overall interface dipole, an important property of the PI atomic species is its electronegativity, i.e. its ability to extract

electron from (or donate electron to) either or both sides of the interface. A simple model of interface dipole can be illustrated as Fig. 4. Elements with larger electronegativities than that of the semiconductor, extracting electron from the semiconductor, form a negative dipole (surface negative, bulk positive), resulting in an increased EA for the ATS and consequently a decreased n-type, and an increased p-type SBH. On the other hand, elements with smaller electronegativities, donating electrons to the semiconductor, otherwise induce a positive dipole (surface positive, bulk negative) therefore decreased EA of the ATS surface along with increased n-type and decreased p-type SBH's are expected.

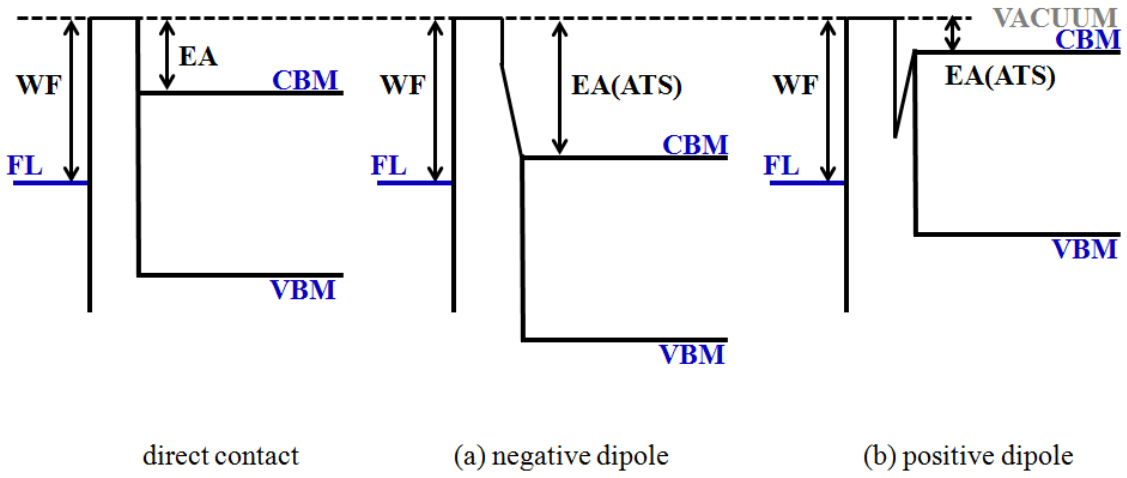

Figure 4. Schematic drawing of shifts in n-type and p-type SBH's with an interface dipole, in the cases of (a) the presence of negative interface dipole, and (b) the presence of positive interface dipole. The directions of SBH shifts according to the change in EA are demonstrated.

Techniques of SBH adjustment by insertion of dipolar organic molecules were reported [54-63], with some remarkable results being obtained. However, preparation of self-assembled molecular structure on semiconductor surfaces and fabrication of reliable metal contacts required special techniques that may be unconventional for semiconductor laboratories, due to the widely

observed low conductivity, insufficient chemical stability and interface non-uniformity that organic molecules may suffer from. Non-organic PI's seem to be more preferable for relatively high stability and conduction, with the perspective of inducing a large dipole moment. Therefore, non-organic PI's were focused on in the present work.

2.3 ATS Surfaces Studied

To form a PI, a precise amount of non-organic adsorbate atoms is first deposited and processed to form an ATS surface, the structure of which is stable enough that it may withstand the subsequent deposition of metal. Silicon (Si) was chosen for its largely known properties and widely spread applications. In addition, adsorbate-terminated Si surfaces such as Si(111)1×1-As [64-71], Si(111)1×1-Cl [72-75] and Si(100)1×1-S [76, 77] were reported to be relatively stable. Studies of SBHs on these ATS surfaces were carried out in our laboratory recently and substantial shifts in SBH have been achieved [53, 78, 79]. This was the thesis work of a fellow graduate student, with substantial assistance and involvement from me. Results from this part of my Ph.D. research, much of which has been discussed at length in Mr. Yang Li's thesis and has also appeared in a few publications that I co-authored, will not be included in this thesis. Only the results of a systematic investigation of the effect of the PI technique on SBH modification with low-electronegativity adsorbates will be included in this thesis. In this investigation, which I am entirely responsible for, results obtained from four ATS surfaces, including the Si(111) $\sqrt{3}\times\sqrt{3}$ -Ga R30°, the Si(111)6.3×6.3-Ga, the Si(111)3×1-K and the Si(100)1×1-Mg, were compared. Schottky diodes were fabricated on above surfaces with the choice of three metals, silver (Ag), gold (Au) and indium (In), for their widely different WF's, the absence of silicide phases in their binary phase diagrams with Si and their relatively low melting points, which

make them suitable for vacuum evaporation. The main results of this investigation are discussed in Chapter 4.

CHAPTER 3. Experiment Setup

Schottky diodes on samples with variable ATS surfaces were fabricated *in-situ* under ultra-high vacuum (UHV) in our laboratory. Subsequent electrical measurements were conducted *ex-situ* under regular vacuum. Details of experimental instruments and typical procedures are described in this chapter.

3.1. UHV ATS Surface Preparation/Characterization/Metallization System

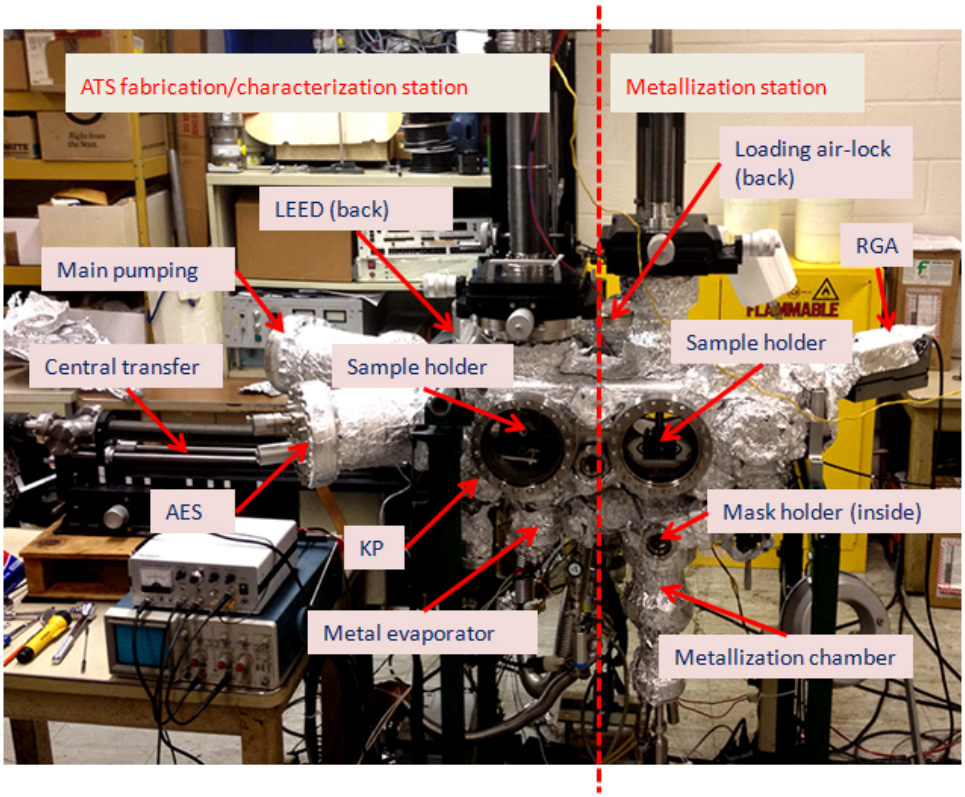

Figure 5. Dual-station UHV system.

A dual-station UHV system (with base pressure in 10^{-10} torr range), powered by a Physical Electronics 300L/sec ion pump, consisting of a loading air-lock, main chamber for ATS surface preparation/characterization and a metal deposition chamber that can be isolated from

main chamber during metal deposition process, was designed and built specifically for the study of ATS surface preparation and *in-situ* Schottky diode fabrication, as shown in Fig. 5. It was made possible to complete the entire sample fabrication cycle without leaving the UHV environment through several specially designed sample transferring/flipping mechanisms. In addition to key components that were commercially available, many features were tailored to our experimental requirements and home-made in the machine shop locally.

3.1.1 ATS Surface Preparation/Characterization Station

ATS surface preparation/characterization station was employed for surface treatment after wet-chemical processing, including formation of clean reconstructed Si surfaces, fabrication of ATS surfaces and common surface characterization capabilities, e. g. low energy electron diffraction (LEED), Auger electron spectroscopy (AES) and Kelvin probe (KP). A sample holder with X-Y-Z-motion, rotation and angular adjustment, accessible via the central transfer mechanism, was designed to bring the sample to essentially every required position, as shown in Fig. 6. Electrical contacts to the sample were made by isolated tantalum clamps for grounding and direct current heating, which also acted as part of locking/unlocking mechanism for sample mounting/releasing. A chromel-alumel thermocouple in contact with the back side of the sample was used to provide simultaneous temperature monitoring. A home-made metal source with an alumina coated tungsten crucible (a commercial SEAS getters alkali metal dispenser was used for K evaporation) was placed underneath the sample holder at the bottom of the UHV chamber for dispensing a small amount of adsorbate atoms on to the surface. A PHI-47 LEED optics and a PHI 11-255G AES analyzer were available for surfaces structure inspection and surface chemical analysis. A Bosecke KP was used for WF measurement, the tip of which could be removed from the path of metal flux as a precaution of contamination.

Figure 6. Sample holder in ATS surface preparation/characterization station.

3.1.2 Metallization Station

Metallization station consisted of a sample mounting/transferring mechanism and an attached vessel that could be isolated during metal deposition, as a consideration to eliminate metal contamination in the main chamber. The sealing, with details described elsewhere [78], was made by two Viton o-rings, which enabled two chambers to work independently. The sample was introduced into metallization chamber through the central transfer mechanism. The sample was brought down to be pressed intimately and firmly by a dual-metal shadow-mask [78], with an array of circular openings of 0.3mm and 2.0mm in diameter, as shown in Fig. 7, against the sample-holder which was maintained at liquid nitrogen (LN2) temperature for preservation of surface structures. Schottky diodes were fabricated through the shadow-mask by direct exposure to metal flux evaporated from a Vecco Knudsen Cell. Thickness of metal pad was manually controllable via deposition duration and calibrated by a crystal monitor adjacent to sample holder. Since there was no external pumping for the metallization chamber, an LN2 cold finger was

utilized as a cold trap. During the metallization process, vacuum levels in the main and the metallization chambers were monitored by a SRS 100 residual gas analyzer (RGA) and an ion gauge, respectively.

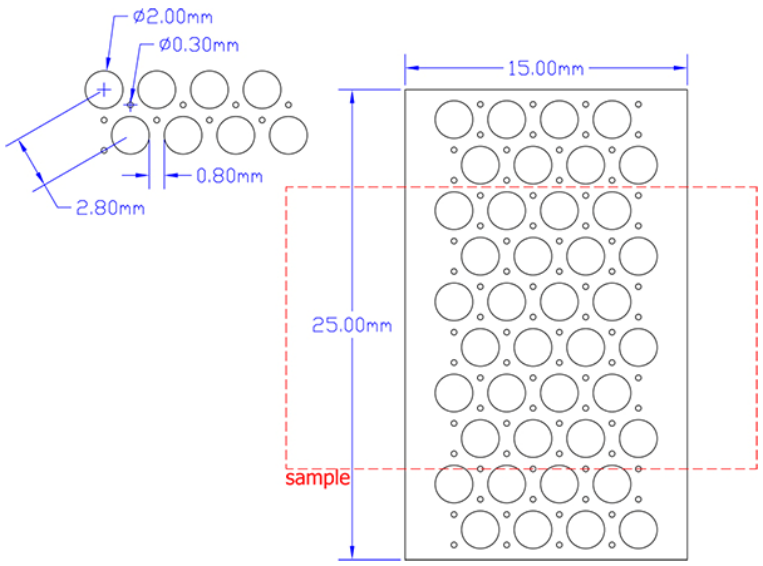

Figure 7. Design of shadow-mask patterns.

3.2. Electrical Measurement Instruments

A Janis ST-500 cryogenic 4-probe station, as show in Fig. 8, for electrical measurements from LN2 (achieved by LN2 cryostat) to room temperature (77-300K) under regular vacuum (~10^{-6} torr) was connected to an Agilent B1500A semiconductor device analyzer, with integrated I-V (B1511A) and C-V (B1520A) modules. Although it was capable of taking 4-probe measurement, only one probe, together with sample holder for back contact, was sufficient for present work. Stiff tungsten probe tips were replaced with copper tips to reduce the damage to diode, without introducing substantial series resistance that may affect the accuracy of our results. Variable temperature I-V and C-V characteristics were obtained via programmable computer interface, with the temperature being controlled automatically by Scientific Instruments 9700

temperature controller. A small portion of present results were taken using our HP 4143 multi-frequency LRC meter and HP 4145B semiconductor parameter analyzer via LabView interfaces.

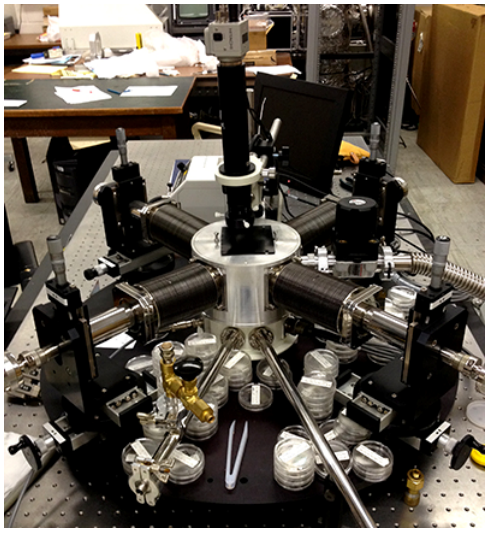

Figure 8. Probe station used for present work.

3.3. Sample Preparation

Si samples, (100) and (111) oriented, both n- and p-type, were used in present work. Samples were cut 0.6”×1.0” in size from either 4” or 6” commercial Si single crystal wafers, with details listed in Table III. Si (100) “epi-wafers” were ideal for present work due to epitaxial grown 5~10μm lightly doped layers on top of 600-700μm thick heavily doped substrates with reduced series resistance and high-quality back ohmic contact, while Si (111) wafers were 500-550μm in thickness with back side treated by ion implantation for ohmic contact. All wafers were pre-coated with photoresist for surface protection.

Table III. Parameters of wafers used for present work.

Orientation	Diameter	Type (Dopant)	Thickness (μm)	Resistance (Ω·cm)	Doping Concentration ($\times 10^{15} cm^{-3}$)
(100)	6”	sub: n (Arsenic) epi: n (Phos.)	sub: 610-640 epi: 10.1-10.9	sub: 0.001-0.003 epi: 1.52-1.68	epi: 2.8-3.2
(100)	6”	sub: p (Boron) epi: p (Boron)	sub: 661-689 epi: 5.5-6.5	sub: 0.01-0.02 epi: 2.5-3.5	epi: 4.0-5.7
(111)	4”	n (Phos.)	500-550	1.3-2	2.4-3.7
(111)	4”	p (Boron)	500-550	1-2	7.1-15.0

Samples received standard RCA cleaning procedures before further surface treatment, ending with formation of Shiraki protective oxide layer [80] on top. The detailed cleaning process was as follows:

(1) Washed in acetone ($CO(CH_3)_2$) with agitation (ultrasonic) to remove protective photoresist;

(2) Rinsed in methanol (CH_3OH) and brushed with Q-tip in diluted Triton solution;

(3) Rinsed in overflowing de-ionized (DI) water for 10 minutes;

(4) Rinsed in methanol for 5 minutes with agitation, then rinsed in acetone;

(5) Boiled in Trichloroethylene (TCE, C_2HCl_3) for degreasing;

(6) Rinsed in acetone, then in methanol;

(7) Dipped in 5% hydrofluoric acid (HF) to remove native oxide, then rinsed in DI water;

(8) Boiled in NH_4OH:H_2O_2:H_2O (1:1:3) solution at 90 ºC in water bath (bring mixture of NH_4OH and H_2O to the temperature first and add H_2O_2 just prior to use) for 10 minutes to form thick surface oxide, followed by (3);

(9) Dipped in diluted HF (2.5%) solution for 15 seconds to remove the oxide, followed by (3);

(10) Boiled in $HCl:H_2O_2:H_2O$ (1:1:3) solution at 90 ºC in water bath (bring mixture of HCl and H_2O to the temperature first and add H_2O_2 just prior to use) for 10 minutes to form thick surface oxide, followed by (3) and (9);

(11) Repeat (8)-(10) if necessary;

(12) Boiled in $HCl:H_2O_2:H_2O$ (3:1:1) solution at 90 ºC in water bath (bring mixture of HCl and H_2O to the temperature first and add H_2O_2 just prior to use) for 10 minutes to form Shiraki oxide layer;

(13) Rinsed and kept in DI water for future use; blow dry with nitrogen (N_2) before use.

3.4. Typical Experimental Procedures

An experiment cycle consisted of the following steps: sample introduction, surface preparation, surface characterization, metallization and electrical measurements. On a typical run, a pre-cleaned sample was first placed in a envelope-like sample holder [78] attached to a magnetic transfer rod in the loading air-lock. After the loading air-lock being pumped down by 2 turbo pumps with a mechanical pump in series to lower 10^{-6} torr, the sample was transferred into ATS preparation/characterization station via transfer mechanisms and mounted onto the sample holder. Hours of degassing at ~350ºC was always required before heating the sample to ~900ºC to remove protective Shiraki oxide layer, forming clean Si(100)2×1 or Si(111)7×7 reconstructed surface. Desired ATS surface was fabricated subsequently and characterized by means of LEED, AES and KP. The sample with ATS surface was released from sample holder, delivered to metallization station by central transfer mechanism, and brought down by LN2 cooled (with the

option of room-temperature) sample holder to lower metallization chamber. Shadow-mask holder was raised to press the sample firmly against the sample holder before metal deposition. Factors such as the temperature of the Knudsen Cell and duration of deposition were optimized according to metal's melting point and vapor pressure at a certain temperature [81]. Once Schottky diodes were made with cell being cooled, the sample was ready to be transferred back into loading air-lock and removed for electrical measurements. If an enhanced back contact was in need, which was once a concern but ruled out later, the sample could be flipped for a thin metal layer to be deposited on the back, with shadow mask completely removed out of the way. Electrical measurements, i.e. variable temperature I-V and C-V were then performed in the probe station. Generally, an over-night pumping down was essential for low temperature measurements.

CHAPTER 4. Formation of ATS Surfaces and Electron Affinities

An ATS surface of high quality was always desired for successful fabrication of Schottky diodes. Generally, clean Si(100)2×1 or Si(111)7×7 surface after Shiraki oxide layer being thermally removed, as a starting point, was required and checked by LEED and AES. As shown by robust and sharp LEED patterns of Fig. 9 (a) & (e), these surfaces were both well ordered and of high quality. Only negligible amount of the common carbon and oxygen contaminants was shown by AES analysis. ATS surfaces were fabricated immediately by dispensing a precise amount of adsorbate atoms onto these clean surfaces at either room temperature or elevated temperatures, followed by low temperature heating treatment, if required, for surface rearrangement.

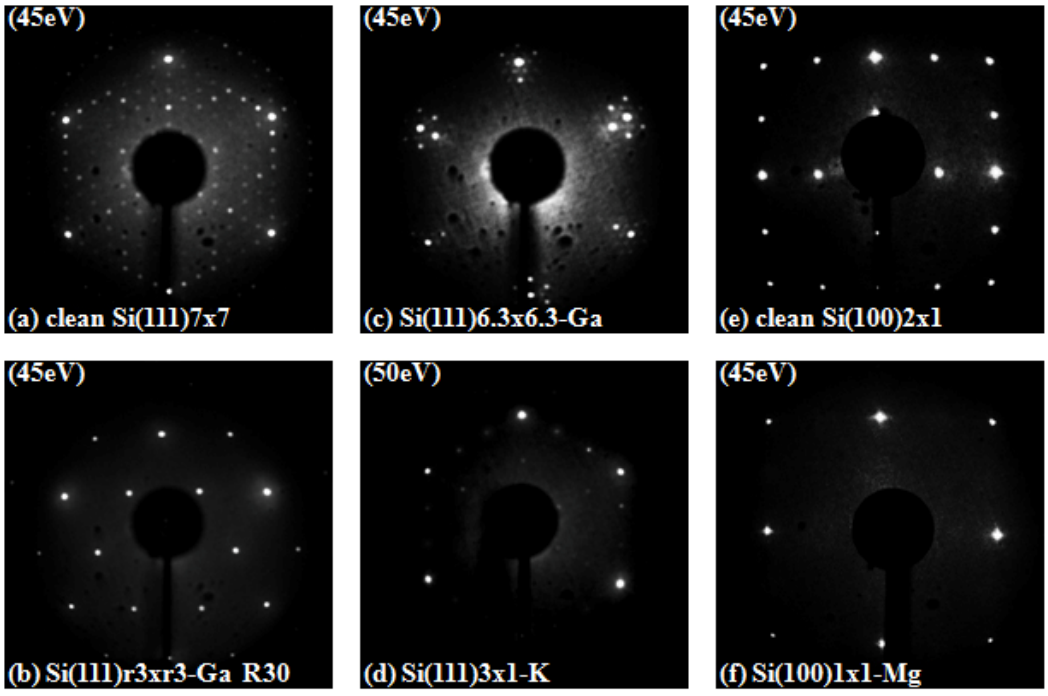

Figure 9. Representative LEED patterns of (a) clean Si(111)7×7, (b) Si(111) $\sqrt{3}\times\sqrt{3}$ -Ga R30°, (c) Si(111)6.3×6.3-Ga, (d) Si(111)3×1-K, (e) clean Si(100)2×1 and (f) Si(100)1×1-Mg surfaces.

4.1 Si(111) $\sqrt{3}\times\sqrt{3}$ -Ga R30° and Si(111)6.3×6.3-Ga Surfaces

Ga, as a trivalent metal, induced superstructures on Si (111) surface have been intensively studied over decades by various groups [82-91], from which two surface reconstructions, Si(111) $\sqrt{3}\times\sqrt{3}$ -Ga R30° and Si(111)6.3×6.3-Ga, as shown in Fig. 10, are known to be relatively stable. When 1/3 monolayer (ML, 1 ML=7.8×10^{14} atoms/cm^2 for Si (111)) of Ga is deposited onto clean Si (111) 7×7surface held at an elevated temperature (~600°C) , the Si(111) $\sqrt{3}\times\sqrt{3}$ -Ga R30° surface reconstruction is formed, in which Ga atoms occupy T_4 sites over the Si double layer and tie up 3 Si dangling bonds per Ga atom[82, 84, 85, 92]. Deposition of ~1 ML Ga at lower sample temperature (~500°C) leads to the formation of Si(111)6.3×6.3-Ga, which is a distinctive incommensurate surface reconstruction, with the top-most Si sites in the Si (111) double layer substituted by Ga atoms, and with excessive Ga atoms weakly bonded to the surface [82, 85]. The unsaturated Si dangling bonds indicate the presence of domain wall, whose atomic and electronic structures are unknown [91]. It has been reported that Ga atoms are mobile on Si (111) surface [92] that at room temperature they tend to form triangular or hexagonal "magic clusters", i.e., islands [85, 93] and steps [93, 94]. These superstructures will not be detectible by LEED, due to a lack of long-range order, and are only observable by direct-space techniques such as the scanning tunneling microscopy (STM). As shown by the robust, sharp LEED patterns of Fig. 9 (b) & (c), both Si(111) $\sqrt{3}\times\sqrt{3}$ -Ga R30° and Si(111)6.3×6.3-Ga surfaces were well ordered and of high quality. After Ga-termination, the intensities of Ga AES signals were consistently observed to be in general agreement with the nominal surface coverage, 1/3 ML for the Si(111) $\sqrt{3}\times\sqrt{3}$ -Ga R30° and ~1 ML for the Si(111)6.3×6.3-Ga, respectively.

Both the Si(111) $\sqrt{3}\times\sqrt{3}$ -Ga R30° and the Si(111)6.3×6.3-Ga surface structures are employed for SBH determination in the present work.

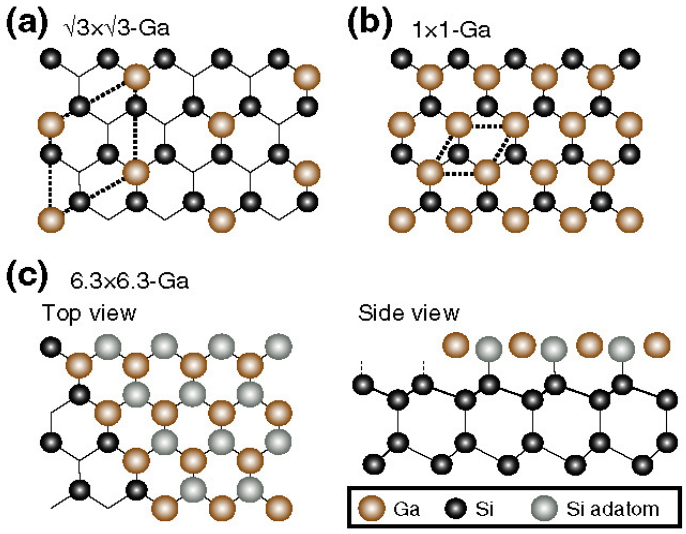

Figure 10. Structural models for the Si(111)-Ga surfaces: (a) $\sqrt{3}\times\sqrt{3}$, (b) 1×1 and (c) 6.3×6.3 reconstructions, top view. (H.W. Yeom, et al.)

4.2 Si(100)1×1-Mg Surface

As a divalent alkaline-earth metal, Mg is an ideal candidate for PI study on Si (100) surface. Starting from clean Si (100)2×1 surface, 2×3, 2×2, a second 2×3 and 1×1 surface structures, as shown in Fig. 11, have been observed at 1/6, 1/3, 1/2 and 1 ML (1 ML=6.8×10^{14} atoms/cm^2 for Si (100)) coverage respectively [95-101]. Si(100)1×1-Mg surface, which is achieved by depositing 1 ML of Mg onto clean Si (100) 2×1 surface at room temperature [97], was chosen for its relative high stability. Robust, sharp LEED pattern in Fig. 9 (f) suggested well ordered surface structure and AES analysis showed intensities of Si and adsorbate signals which were in general agreement with the nominal surface coverage, 1 ML for Si(100)1×1-Mg surface. One notes in passing that at the same surface coverage (1ML), a 2×1 reconstruction has also

been proposed [102] by DFT first-principles calculation as the minimum energy configuration. In actual experiments in our laboratory, the unreconstructed 1×1 was observed, thus the 2×1 was not considered as the surface structure for 1 ML Mg coverage in the present work.

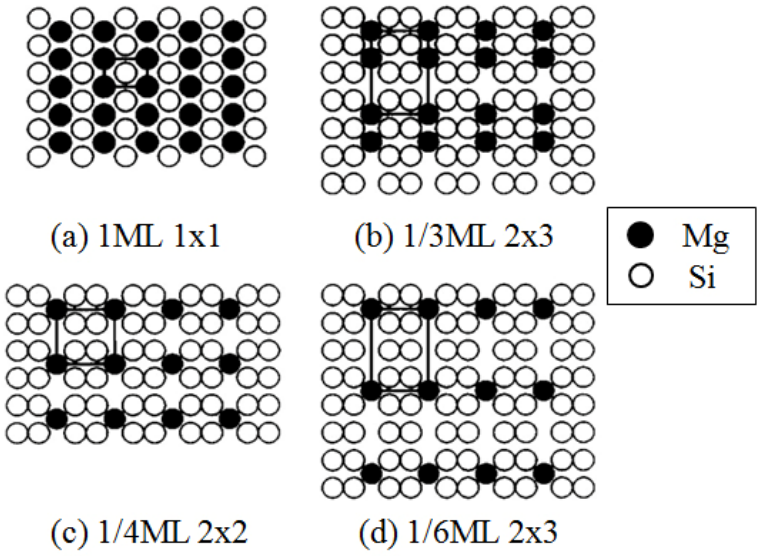

Figure 11. Structural models for the Si(100)-Mg surfaces: (a) 1×1, (b) 2×3, (c) 2×2 and (d) 2×3 reconstructions, top view. (Y. Kawashima, et al.)

4.3 Si(111)3×1-K Surface

Among monovalent alkali metals, K has a diffusivity far lower than that of Na and Li in Si, for its ionic radius (1.33Å) exceeds the covalent radius (1.17Å) of Si [103]. Si(111)3×1-K surface, as shown in Fig. 12, has been extensively studied [104-114], and it is obtainable by deposition of K onto clean Si(111)7×7 surface followed by a short annealing at ~500°C[115]. Despite long debate about surface coverage for this alkali-metal induced structure [104, 106, 108, 111-113], angle-resolved ultraviolet photoelectron spectroscopy and x-ray photoelectron spectroscopy studies showed that only 1/3 of Si dangling bonds are terminated by K atoms, while other dangling bonds make π-bonded chain [115]. Surface coverage for Si(111)3×1-K structure

is nominally 1/3 ML. DFT calculations also demonstrated that K atoms prefer to occupy T4-type lowest energy sites, but with a high probability to migrate to H3-type and B2-type positions with similar adsorbing energies [92], resulting in a unstable surface structure. Sharp LEED pattern in Fig 9 (d) suggested that the Si(111)3×1-K structure was well formed and the ratio of intensities of Si and adsorbate AES signals was in general agreement with the nominal surface coverage, 1/3 ML for Si(111)3×1-K surface.

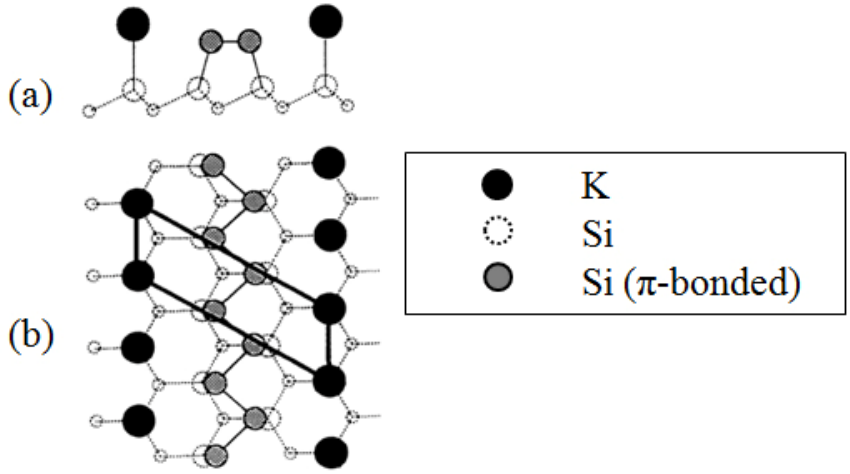

Figure 12. Structural model for the Si(111)3×1-K, (a) side view and (b) top view. (K. Sakamoto, et al.)

4.4 Electron Affinities of ATS Surfaces by KP Measurement

The change in the EA of the Si surface through the use of the adsorbates is the mechanism by which the PI technique is envisioned to shift the SBH. Here, the EA's of the ATS surfaces are inferred from in-situ KP measurements. What KP measures is actually the contact potential difference (CPD), or the relative WF of the target surface with respect to that of the reference tip of KP, gold, which should be kept free of contamination/adsorbates. It should be mentioned that a shift in WF is suggestive of, although not equivalent to, a similar shift in EA,

due to a possible shift in the FL position in the gap between the ATS and the clean Si surface. To actually deduce the EA of a particular ATS surface from WF data, one needs information about its surface FL position, which for these ATS surfaces is largely unknown. To circumvent these difficulties, KP measurements were carried out on both n- and p-type samples and with heavily doped Si substrates. Heavily doped substrates were chosen for their FL's are located in the vicinity of either conduction band minimum (CBM) for n-type or valence band maximum (VBM) for p-type substrate.

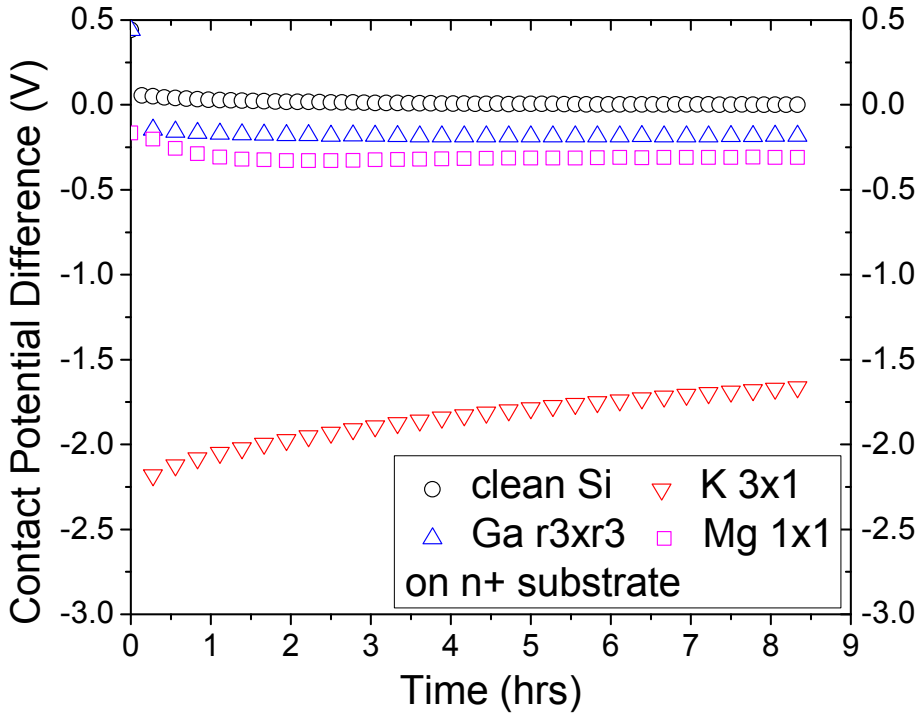

Figure 13. CPD measured by KP on K-, Mg- and Ga-terminated surfaces with reference to clean Si surface on heavily doped n-type substrates.

To minimize systematic errors and difficulties associated with absolute WF measurement in UHV [116, 117], measurements were always conducted in tandem for two different surface structures fabricated on the same substrate, with the emphasis placed on the difference between the two measurements. More specifically, the WF of an ATS surface was first measured,

followed by the measurement of the clean reconstructed Si surface obtained on the same substrate by desorbing adatoms at ~900°C. The differences between these back-to-back measurements are referred as a new CPD, surface potential of ATS surface with reference to that of corresponding clean surface, which is actually equivalent to the shift in WF. CPD's obtained on Si(111)$\sqrt{3}\times\sqrt{3}$ -Ga, Si(111)6.3×6.3-Ga, Si(111)3×1-K, and Si(100)1×1-Mg surfaces for n+ substrates were displayed in Fig. 13.

Table IV. Work function/electron affinity of ATS surfaces studies in the present work.

WF or EA (eV)	$\Delta\phi$ (n-type)	$\Delta\phi$ (p-type)	$\Delta\chi$ (expt.)	$\Delta\chi$ (ref.)
Si(111)$\sqrt{3}\times\sqrt{3}$ -Ga	-0.26	-0.20	(-0.23)	-0. 40
Si(111)6.3×6.3-Ga	-0.33	-0.22	(-0.27)	-
Si(100)1×1-Mg	-0.32	-0.35	(-0.33)	-
Si(111)3×1-K	-1.66	-1.58	(-1.62)	(-1.4)

From the KP measurement, the WF of the clean Si surface was consistently measured to be independent of substrate doping. This is in agreement with the fact that the FL is firmly pinned at 0.63eV above VBM [118] on Si(111)7×7 surface. As shown in Fig. 13, on Ga-terminated Si (111) $\sqrt{3}\times\sqrt{3}$ R30° surface the WF was decreased by 0.25 eV. For reference, the EA for the Si(111)$\sqrt{3}\times\sqrt{3}$ -Ga R30° surface has been theoretically calculated to be ~ 0.4 eV lower than that for clean Si(111)7×7 [119]. WF on Si(111)3×1-K surface underwent a huge drop of ~1.6eV compared to that of clean Si(111)7×7 surface. This is close to previous photoemission result, ~1.4eV, given by Sakamoto et al [115]. Interestingly, an aging effect was seen as the WF of Si(111)3×1-K surface increased gradually by ~0.7eV after 8 hours. Similar phenomenon has been observed by Ditzinger et al. [105] on K covered Si (111) surface (with no specified surface

structure mentioned) by photoemission, as WF increased by ~0.8eV after 12 hours, which was attributed to residual oxygen contamination on surface. WF of Si(100)1×1-Mg surface, which was unavailable in literature, was found ~0.3eV lower than that of clean Si(100)2×1 surface. These results are in agreement with positive dipole formation and resultant decrease in WF, expected of the charge transfer from adsorbate atoms to Si, according to PI method. The substantial shift in WF, in the absence of information on the surface FL position, was interpreted as reflecting a shift in the EA of the same magnitude. The changes in WF ($\Delta\phi = \phi_{ATS} - \phi_{clean}$) and suggested changes in EA ($\Delta\chi = \chi_{ATS} - \chi_{clean}$) obtained on the above ATS surfaces are summarized in Table IV, with reference with the values available in literature.

CHAPTER 5. Modification of Schottky Barrier Height on Si (111) By Ga-termination

In this chapter, SBHs for Ag, Au and In on Si(111) $\sqrt{3}\times\sqrt{3}$ -Ga R30° and Si(111)6.3×6.3-Ga surfaces are studied and found to be shifted by as much as 0.2eV from those on clean Si(111)7×7, in the same direction as the observed EA shift for the ATS surface. These results are thus in agreement with the expected Ga to Si charge transfer and illustrate the general validity of the PI technique. However, large degrees of SBH inhomogeneity are observed for diodes on Ga-terminated surfaces, likely due to insufficient stability of these surfaces to withstand metal interaction.

5.1 Results

As shown by the robust, sharp LEED patterns of Fig. 9, the clean Si(111)7×7 surface and the Si(111) $\sqrt{3}\times\sqrt{3}$ -Ga R30° and Si(111)6.3×6.3-Ga surfaces were all well ordered and of high quality. AES analysis showed negligible amount of the common carbon and oxygen contaminants for the clean Si(111)7×7. After Ga-termination, the intensities of Ga AES signals were consistently observed to be in general agreement with the nominal surface coverages, 1/3 ML for the Si(111) $\sqrt{3}\times\sqrt{3}$ -Ga R30° and ~1ML for the Si(111)6.3×6.3-Ga. KP measurements on both n- and p-type doped Si showed that both the Si(111) $\sqrt{3}\times\sqrt{3}$ -Ga R30° and the Si(111)6.3×6.3-Ga surfaces had a WF smaller than that for the clean Si(111)7×7 by ~ 0.25-0.30 eV. Variable temperature I-V curves of Ag, Au and In on clean 7×7 (left) and Si(111) $\sqrt{3}\times\sqrt{3}$ -Ga R30° (right) surfaces for both n-type (upper) and p-type (lower) Si are displayed in Fig. 14-16.

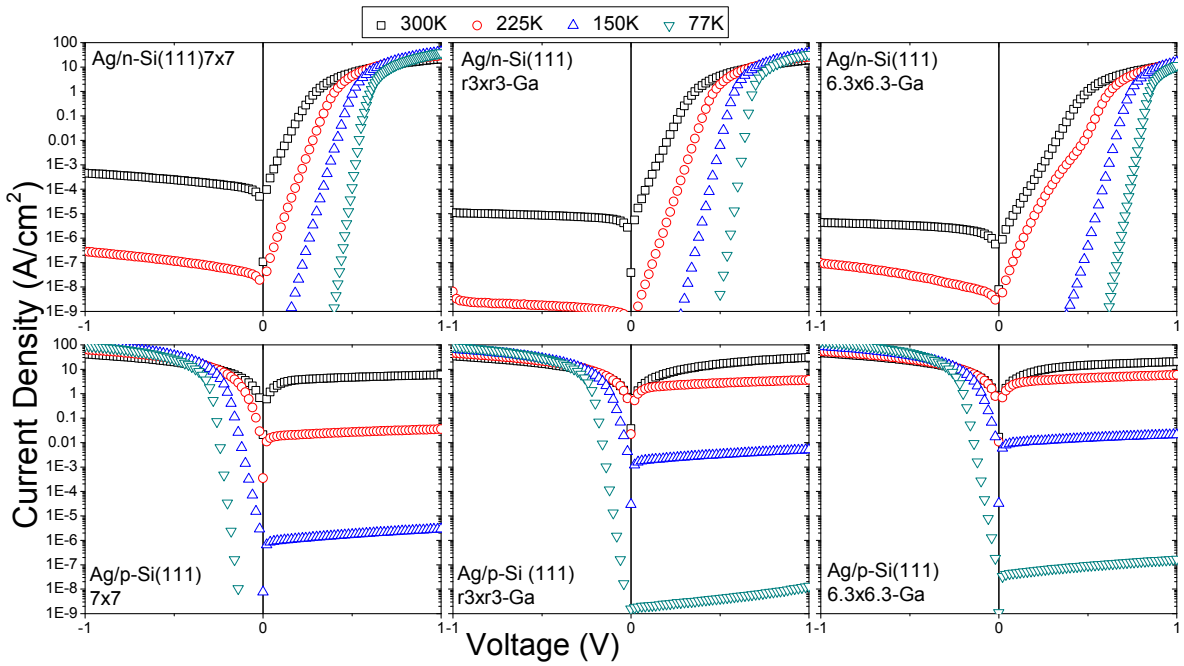

Figure 14. I-V characteristics of Ag on clean Si(111)7×7, Si(111) $\sqrt{3}\times\sqrt{3}$ *-Ga R30° and Si(111)6.3×6.3-Ga surfaces at variable temperatures.*

Saturation current densities deduced from linear portion of the forward current densities were used to calculate the SBH from the thermionic-emission equation (for uniform SBH) and recorded in Table V. From these analyses, an increase in the n-type Ag SBH for either of the Ga-terminated surfaces by ~0.10-0.15 eV over that for the clean Si(111)7×7 was found, with a similar decrease for the p-type interfaces.

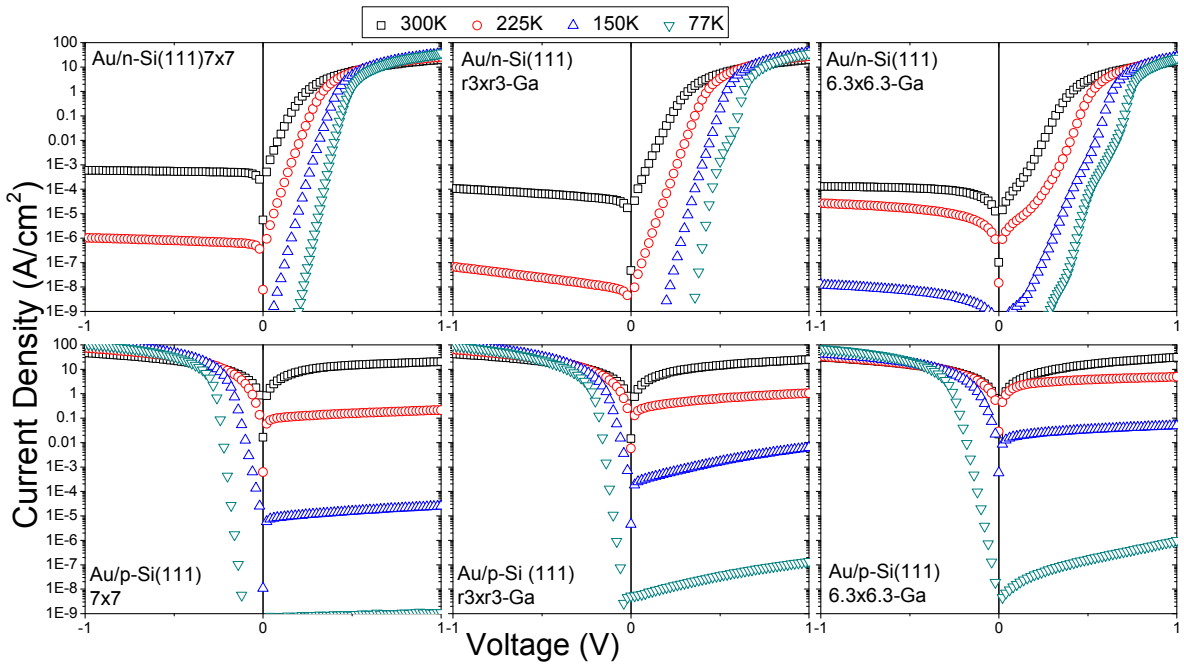

Figure 15. I-V characteristics of Au on clean Si(111)7×7, Si(111) $\sqrt{3}\times\sqrt{3}$ *-Ga R30° and Si(111)6.3×6.3-Ga surfaces at variable temperatures.*

The directions of the SBH shifts were in agreement with theoretical prediction by PI method based on the expected electron transfer from Ga to Si. For the Au and In diodes, SBH shifts in the same respective directions as Ag were found, although the magnitudes of the SBH changes were not as significant, ~ 0.05-0.10 eV. Even though the forward-bias I-V curves had nearly linear characteristics over many decades, ideality factors were consistently greater than unity, typically 1.05-1.4 for Ag and 1.1-2.0 for Au and In. "Leakage component" could also be observed occasionally at low temperature. Interestingly, the current level at large forward biases (~0.8V-1.0V) was higher at an intermediate temperature of 150K than at any other temperature. This dependence was not unexpected, because in this bias range, the current flow was dominated by the series resistance across the Si substrate, and the bulk resistivity of Si with 10^{15} doping levels had a minimum in the 100-150K temperature range [120]. However, the actual

observation of this expected temperature-dependence indicated that the back ohmic contact was of high quality.

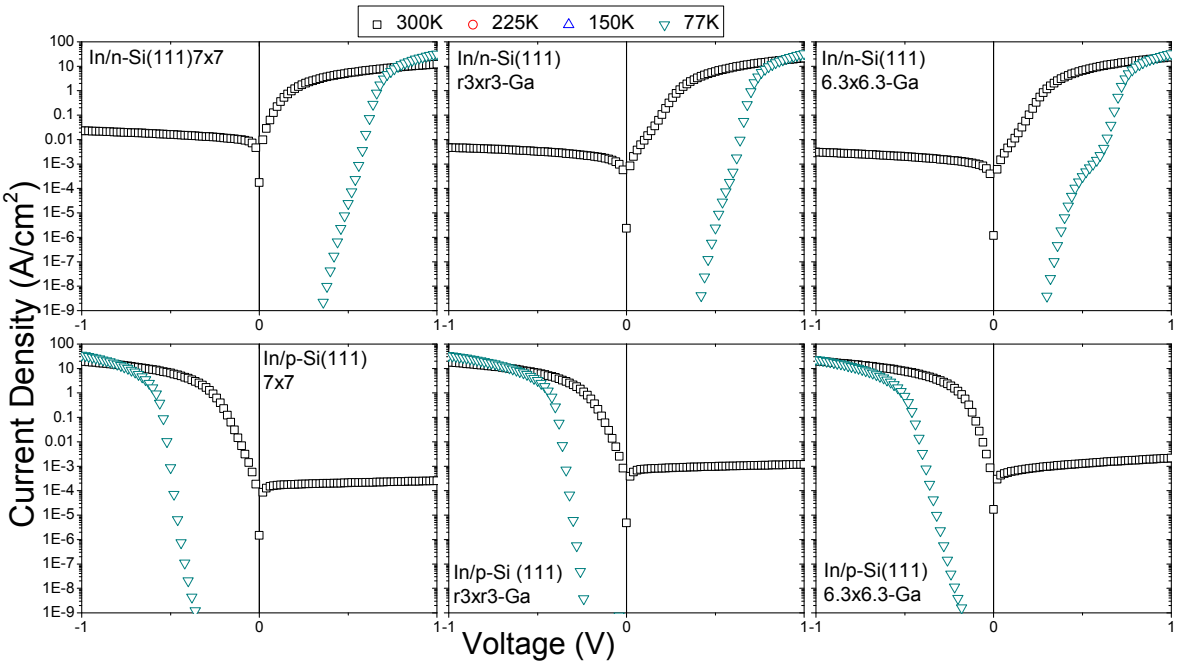

Figure 16. I-V characteristics of In on clean Si(111)7×7, Si(111) $\sqrt{3}\times\sqrt{3}$ *-Ga R30° and Si(111)6.3×6.3-Ga surfaces at variable temperatures.*

The slopes of the Richardson's plots of the saturation currents from all interfaces, shown in Fig. 17-18, essentially corroborated SBH trends deduced from individual temperatures, although the magnitudes of A-E deduced SBH tended to be slightly less than the I-V results. The active conducting areas rendered from intercepts of Fig. 17-18, based on pure thermionic-emission, were consistently found to be less than the geometrical dimension of the diodes. Furthermore, there was a slight curvature in the Richardson's plots, showing that the operative SBH decreased for the lower temperatures.

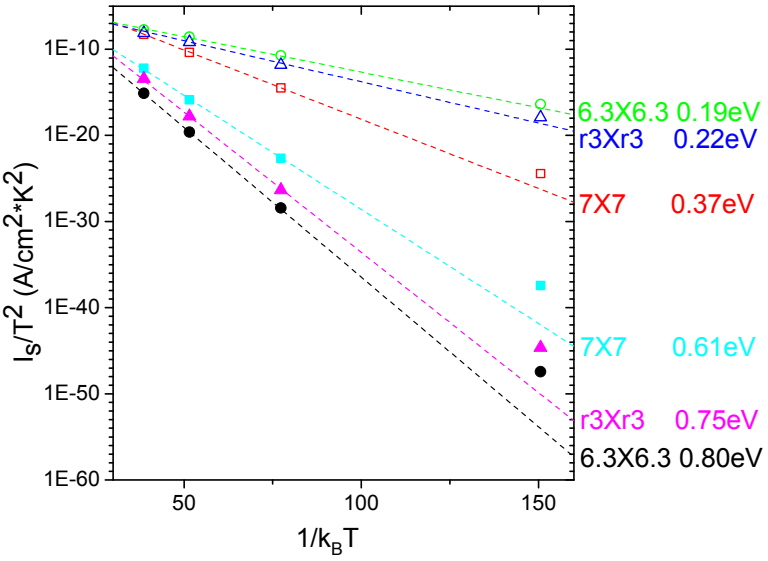

Figure 17. Richardson's A-E plots of Ag SBH's measured on clean and Ga-terminated Si (111) surfaces.

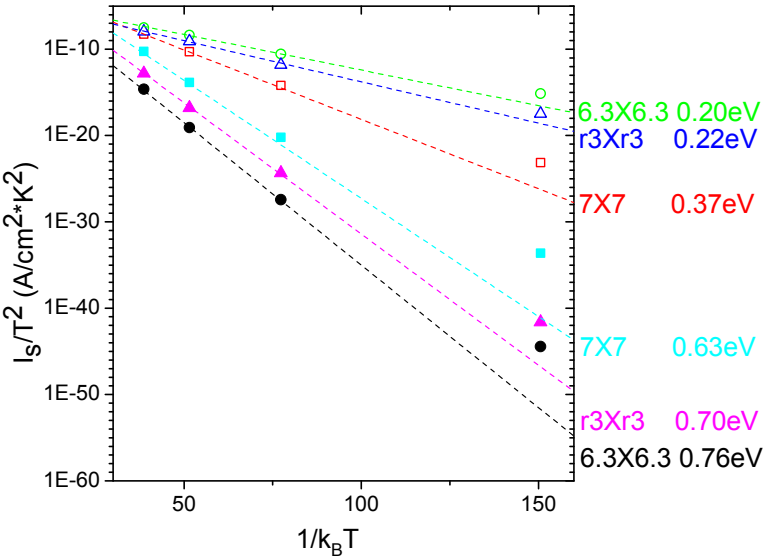

Figure 18. Richardson's A-E plots of Au SBH's measured on clean and Ga-terminated Si (111) surfaces.

C-V plots in Fig. 19-21 showed the same SBH trends as those seen from I-V and A-E measurements, although SBH values deduced from C-V invariably exceeded I-V results by

considerable amounts. Parallel C-V curves in Fig. 19-21 showed no change in the doping level when Ga-terminated surfaces were used. From all results summarized in Table V, an SBH shift of 0.1eV~0.2eV, due to Ga, could be concluded for all three metals studied.

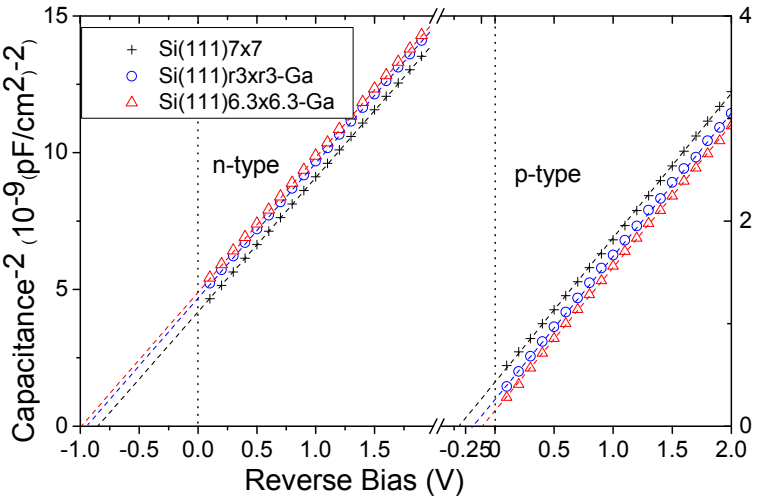

Figure 19. C-V plots of Ag SBH's measured on various Ga-terminated Si (111) surfaces at 77K and 400 kHz.

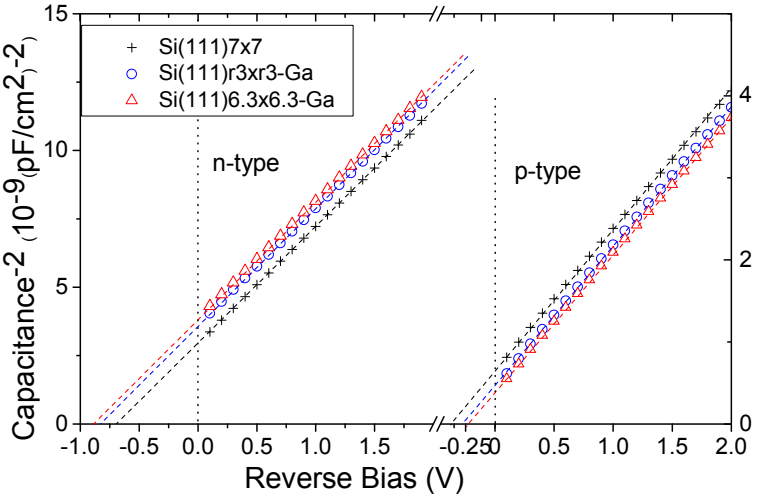

Figure 20. C-V plots of Au SBH's measured on various Ga-terminated Si (111) surfaces at 77K and 400 kHz.

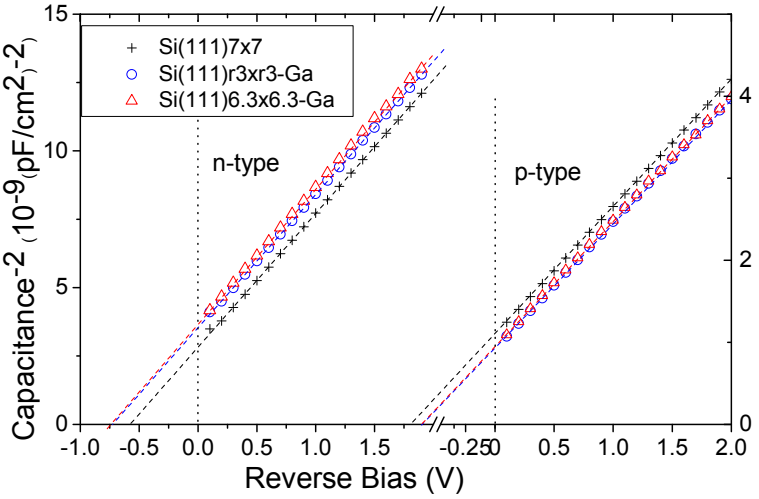

Figure 21. C-V plots of In SBH's measured on various Ga-terminated Si (111) surfaces at 77K and 400 kHz.

5.2 Discussion

Non-ideal characteristics, e.g., leakage component in I-V, greater-than-unity ideality factor, lower A-E deduced SBH, curvature in Richardson plots, and the dependence of SBH on techniques of measurement dominated the junction characteristics presently observed and are a clear indication that all the MS interfaces presently studied had inhomogeneous SBH. Under these circumstances, a complete description of the SBH of the interface should reflect the fact that the SBH is inhomogeneous. Following this logic, the SBH values listed in Table V are given with significant ranges. Each entry represents the range of inhomogeneous SBH observed from the diodes studied for a particular MS interface and with a particular measurement technique. As the sensitivity for SBH inhomogeneity varies with the measurement technique, the range of the SBH also varies. However, these ranges were unrelated to the accuracy of the measurements, but simply manifested the non-uniform nature of the interface under study. The difference between the SBH ranges, for I-V and AE, presently reported and the size of error bars for SBH typically

Table V. Summary of measured SBH by I-V, C-V and A-E methods, with deduced ideality factor. Note that all data are presented as a range to demostrate the dominating effect of SBH inhomogeneity.

SBH (eV)			clean Si(111) 7×7	Si(111) $\sqrt{3}\times\sqrt{3}$ -Ga	Si(111) 6.3×6.3-Ga
Ag	n-type	I-V	0.653~0.715	0.735~0.826	0.723~0.854
		n	1.25~1.03	1.29~1.03	1.37~1.08
		A-E	0.58~0.65	0.63~0.76	0.68~0.80
		C-V	0.709~0.789	0.874~0.937	0.859~0.965
	p-type	I-V	0.336~0.375	0.234~0.252	0.209~0.231
		n	1.21~1.06	1.26~1.05	1.39~1.11
		A-E	0.32~0.36	0.22~0.25	0.18~0.21
		C-V	0.387~0.464	0.272~0.352	0.232~0.294
Au	n-type	I-V	0.620~0.736	0.734~0.780	0.695~0.793
		n	1.41~1.09	1.69~1.05	1.92~1.16
		A-E	0.51~0.63	0.63~0.70	0.61~0.75
		C-V	0.723~0.810	0.779~0.925	0.771~0.932
	p-type	I-V	0.310~0.365	0.211~0.232	0.203~2.210
		n	1.19~1.04	1.47~1.03	1.72~1.06
		A-E	0.29~0.37	0.18~0.22	0.18~0.20
		C-V	0.351~0.425	0.260~0.343	0.239~0.346
In	n-type	I-V	0.481~0.543	0.545~0.602	0.530~0.651
		n	1.30~1.12	1.44~1.09	1.75~1.11
		C-V	0.582~0.646	0.651~0.792	0.673~0.785
	p-type	I-V	0.475~0.503	0.344~0.385	0.338~0.390
		n	1.22~1.05	1.53~1.04	1.61~1.06
		C-V	0.589~0.605	0.471~0.527	0.454~0.556

reported in the literature should be stressed. Traditionally in the literature, the SBH of a particular MS interface is reported singularly as an average, even when evidence for SBH inhomogeneity abounded. Any spread in the SBH reported then reflected the variation of the "average SBH" among different diodes. Presently, the range of SBH in Table V is that observed usually for every diode studied in a particular category. Only the C-V SBH results from Table V can be directly compared with SBH values of the literature, because the C-V measurement technique is insensitive to the presence of SBH inhomogeneity. Selected I-V characteristics in the present investigation were explicitly analyzed with thermionic emission theory for

inhomogeneous SBH [34, 38]. Fig. 22 is an example of such an analysis applied to a Au diode formed on n-type Si(111) $\sqrt{3}\times\sqrt{3}$ -Ga R30° surface. Experimentally obtained I-V characteristics at different temperatures (symbols) were adequately reproduced by I-V forward current calculated with Eq. (22).

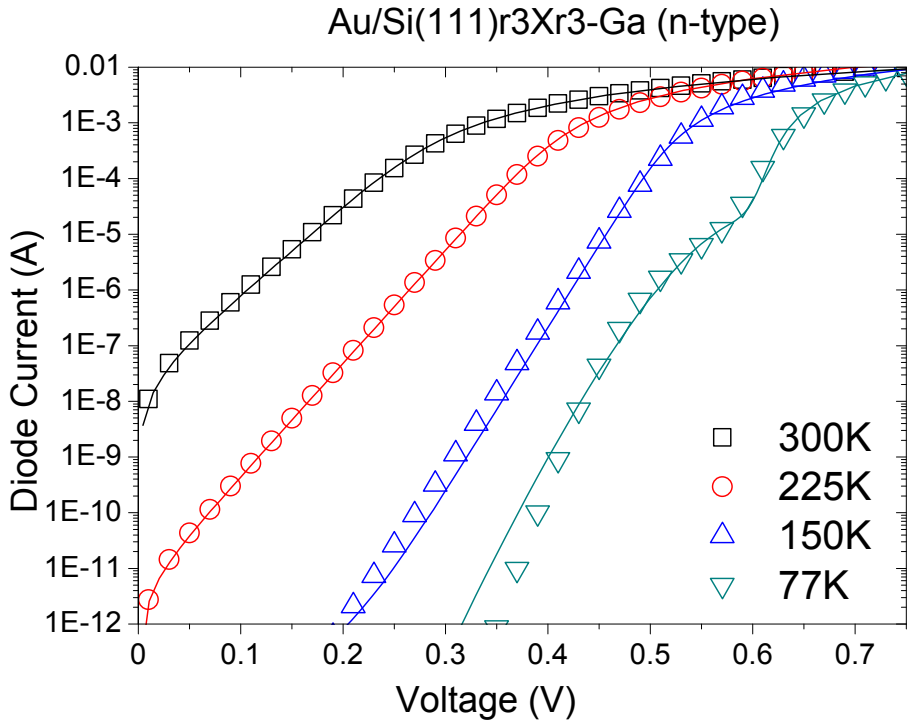

Figure 22. Actual (dots) and calculated (lines) I-V characteristics of Au on n-type Si(111) $\sqrt{3}\times\sqrt{3}$ *-Ga R30° surface, with an area of* 7.07×10^{-4} cm^2 *and an uniform SBH of 0.85V which contains a low SBH patch with* $c_1=4\times10^{-12}$ *and* $\gamma_0=1.01\times10^{-3}$ $V^{1/3}cm^{2/3}$.

For this particular diode, a uniform background SBH Φ_B^0=0.85eV was assumed, which contains sharply distributed low-SBH patches [34] with density $c_1=4\times10^{-12}$ and strength $\gamma_0=1.01\times10^{-3}$ $V^{1/3}cm^{2/3}$. Note that the apparent low-SBH component at 77k and the temperature dependence of the ideality factor were both simulated by this analytic model of electron transport at inhomogeneous SB.

Since it has been previously demonstrated experimentally and theoretically that the SBH varies with the atomic structure of the MS interface [3, 4, 24, 35, 37, 121], the presence of inhomogeneous SBH for the interfaces presently studied can be attributed to locally varying interface structure. At an interface between metal and clean Si (111), the variation of the SBH is due to variables such as the orientation of the metal crystallite, incommensurate structure within a metal crystal, and interface compound formation, that involve only atoms of the metal and Si. When a metal junction is formed with Ga-terminated Si surface(s), the range of atomic structure present at the interface is significantly widened. Not only may the variables mentioned above be operative, but non-uniformity involving the Ga coverage, such as incomplete coverage, Ga islanding, binary or ternary Ga-containing compound formation, may also be present. While direct structural information of the inhomogeneous interfaces is unavailable, we examine the implications on interface uniformity that can be drawn from electrical data alone. As suggested by Fig. 14 and the range of ideality factors shown for various interfaces in Table V, the extent of SBH inhomogeneity on Ga-terminated Si seems smaller for Ag interfaces than for interfaces with Au and In. A plausible explanation of this difference in behavior may be the reduced interaction between Ag and Ga-terminated Si surface [53] because of the similarity in their Pauling electronegativities: 1.93 (Ag), 1.81 (Ga) and 1.90 (Si) [122]. Au has a significantly higher electronegativity of 2.4, suggesting higher reactivity with Ga and Si. In has only a slightly lower electronegativity of 1.78, but has a very large bond energy with Si compared with the In-Ga bond energy (462.8±21kJ/mol vs. 94±3 kJ/mol) [122], perhaps making the break-up of the Ga-terminated surface structure easier. The observed smaller degree of SBH non-uniformity for Ag seems consistent with simple thermodynamic analysis of the stability of the Ga-terminated surface structure in the presence of these metals. For reference, the bond dissociation energies at

298K for Ag-Si, Ag-Ga Au-Si, and Au-Ga are 185.1±9.6 kJ/mol, 159±17 kJ/mol, 304.6±6.0 kJ/mol, and 290±15 kJ/mol, respectively [122].

The observed decrease in the EA of the Ga-terminated surfaces from that of the clean Si (111)7×7 is in agreement with the positive surface dipole of these ATS surfaces. According to the PI mechanism, Eq. (25), the n-type SBH should be higher on Ga-terminated surface(s) from that on the clean Si surface. Indeed, experiments showed that, for each of the metals, the n-type SBH was higher, and the p-type SBH lower, than that on the clean Si surface. However, the magnitude of the observed SBH shift was smaller than that predicted by the PI method, ~0.25-0.3 eV, especially for Au and In. For Ag, the amount of SBH shifts by C-V measurement, ~0.15 eV, came close to the effect suggested by PI. Strictly speaking, the PI method is only valid under the following two conditions: (a) the partisan interlayer remains uniformly over the entire interface and (b) adsorbate atoms are "partisan" to the silicon and have little interaction with the metal. In view of discussion above, the Ga-terminated structure may not be inert against metal reaction, which may partially break up the Ga-Si bonds and reduce the dipolar effect of the interlayer. According to analyses above, among the three metals used, Ag has the smallest tendency to react with the Ga-terminated structure. It is therefore not surprising that the magnitude of SBH adjustment was the largest for Ag. At the final interfaces, especially for Au and In, the directional Ga-Si bonds are likely partially destroyed or modified. Because of the large difference in chemical natures of Au, Ag, and In, there could be new directional bonds formed which could influence the local SBH. Presently observed SBH shifts and levels of SBH inhomogeneity are consistent with the incomplete nature of the Ga-terminated surface structure at the final MS interface. Furthermore, more of the directional Ga-Si bonds seem to have survived at the Ag junction than at the Au or In junction. However, the overwhelming

experimental finding of the present study is that these SBH shifts, even though of magnitudes less than predicted by a strict application of the PI rule, were still quite significant and were in directions proposed by the PI mechanism. Therefore, the basic capability of shifting the SBH of Si in both directions, through the use surface adsorbates with electronegativities larger and smaller than Si, that the PI method set out to achieve, has indeed been demonstrated.

Finally, we address the possibility that SBH shift could be due to the formation of heavily doped Si layer near the MS interface, instead of interface dipole adjustment. This issue arises because it is known that a thin layer of Si at the MS interface which has been contaminated or accidentally doped p-type with high concentration, could produce a sizeable increase in the n-type SBH and decrease in the p-type SBH [123-125]. The possibility exists that Ga, as a p-type dopant for silicon, could have diffused into bulk silicon to create a p+ layer in the depletion region near the interface. However, this possibility can be safely ruled out as having any relevance for the present results. First of all, the depletion region doping concentration, deduced from C-V plots shown in Fig. 19-21, showed no evidence for changed doping profile. More importantly, the total Ga diffusion length for the heat treatment used in these experiments can be estimated to be less than 2×10^{-10} cm based on known bulk diffusivity [126], whereas to produce the ~0.1-0.2 eV SBH shift by doping, a ~10^{19} cm^{-3} p-type doped layer with a thickness of ~4-5nm would be required [12, 125].

5.3 Summary

The SBH of Ag, Ag and In on Ga terminated Si(111)$\sqrt{3}\times\sqrt{3}$ -Ga R30° and Si(111)6.3×6.3-Ga surfaces have been studied in detail. Substantial increases in n-type SBH and decreases in p-type SBH, by as much as 0.2eV, were generally deduced from various techniques,

in agreement with the expectation of the PI method. Combined with SBH results previously found on As-, Cl- and S-terminated surfaces[53, 79], the present work demonstrated a wide range of SBHs on Si accessible with the PI approach, and also shed light on the formation mechanism of the SBH. However, all interfaces presently investigated, including those on Ga-terminated and clean Si surfaces, were found to have inhomogeneous SBH. This is a very common feature of most non-epitaxial MS interfaces [4, 34, 127, 128], and is an issue that needs to be dealt with in the development of SBH tuning technologies. For the PI method, the present work showed that the chemical stability of the metal-ATS interface was important for the effectiveness of this approach.

CHAPTER 6. Schottky Barrier Height Modification with K and Mg Partisan Interlayer

In this chapter, alkali and alkaline-earth metals are used as adsorbates on Si to create more reactive surfaces. SBH's for Ag, Au and In on Si(111)3×1-K and Si(100)1×1-Mg surfaces are studied and observed to be shifted by as much as ~0.15eV from that on clean silicon surfaces, in the expected direction, thus showing the general validity of the PI technique. However, significant levels of SBH inhomogeneity are observed and the strength of the PI effect is reduced, likely due to interaction of these surfaces with metal. The present work completes the systematical study of the PI effect by employing monovalent and divalent metals as the surface adsorbate.

6.1 Results

Variable temperature I-V curves of Ag, Au and In on clean Si(111)7×7 (left) and Si(111)3×1-K (right) surfaces for both n-type (upper) and p-type (lower) are displayed in Fig. 23-25. These curves were analyzed with the thermionic-emission equation (for uniform SBH) by deducting saturation current densities and ideality factors from linear portion of the forward current densities. SBH's calculated from these data were recorded in Table VI.

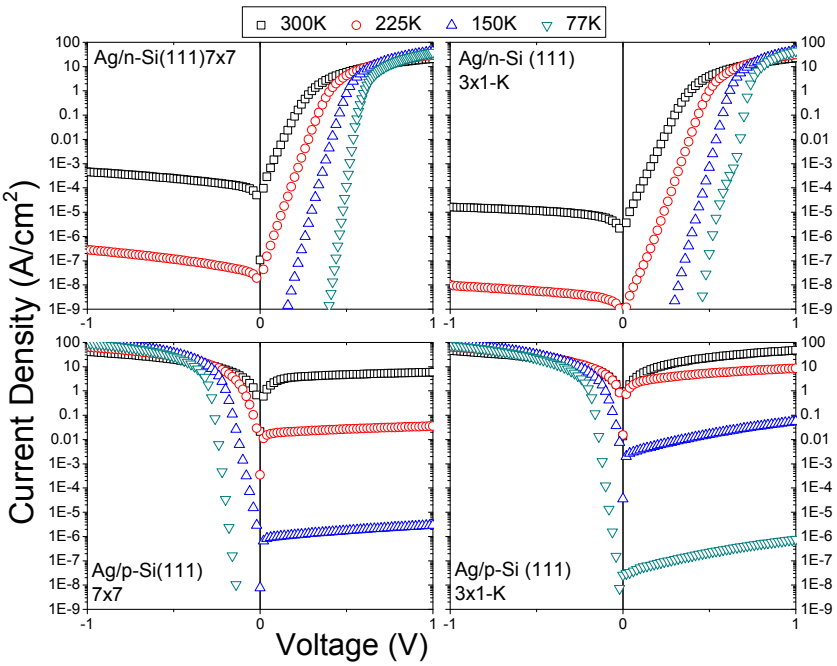

Figure 23. I-V characteristics of Ag on clean Si(111)7×7 and Si(111)3×1-K surfaces at variable temperatures.

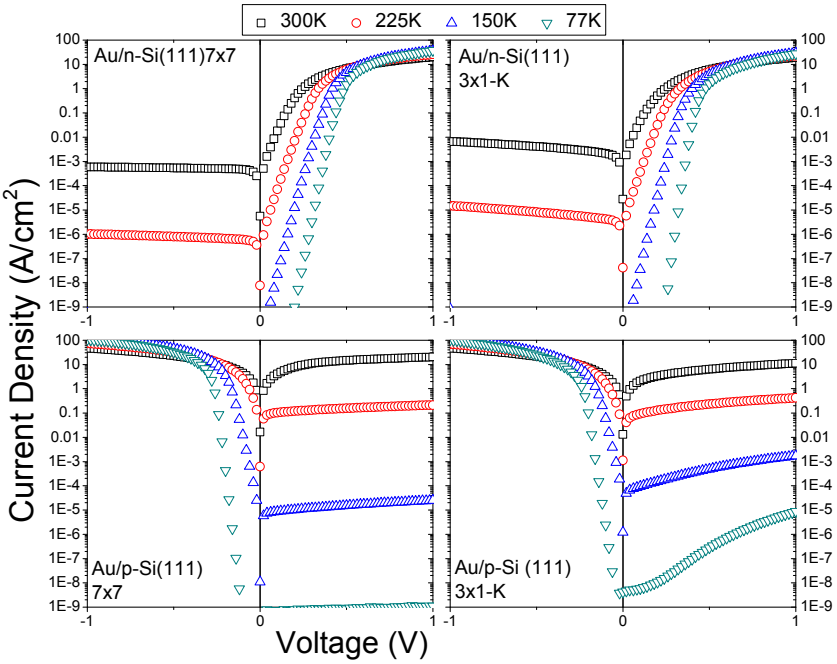

Figure 24. I-V characteristics of Au on clean Si(111)7×7 and Si(111)3×1-K surfaces at variable temperatures.

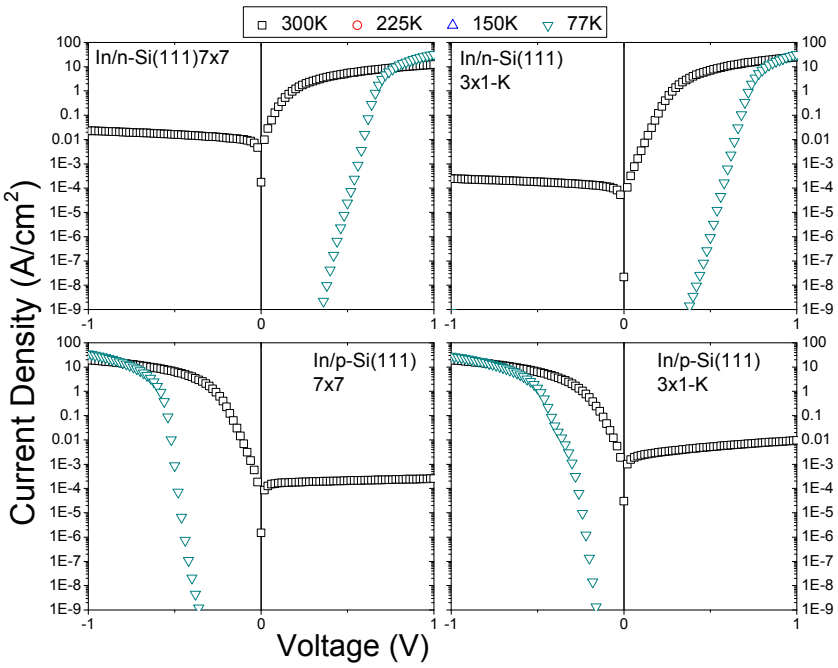

Figure 25. I-V characteristics of In on clean Si(111)7×7 and Si(111)3×1-K surfaces at variable temperatures.

An increase in the n-type Ag SBH for Si(111)3×1-K surface by ~0.10-0.15 eV over that for the clean Si(111)7×7 was found, with a decrease for the p-type SBH. For the Au and In diodes, SBH shifts in the same respective directions as Ag were found. However, for n-type Au SBH, such effect was less significant, likely attributed to unstable surface and resulting inhomogeneous SBH. Similar trend was also demonstrated by I-V characteristics of Ag, Au and In SBH on clean Si(100)2×1 and Si(100)1×1-Mg surfaces as shown in Fig. 26-28, with a SBH shift of ~0.20-0.25 eV. The directions of the SBH shifts were in agreement with theoretical prediction by PI method based on the expected electron transfer from elements with smaller electronegativities to Si.

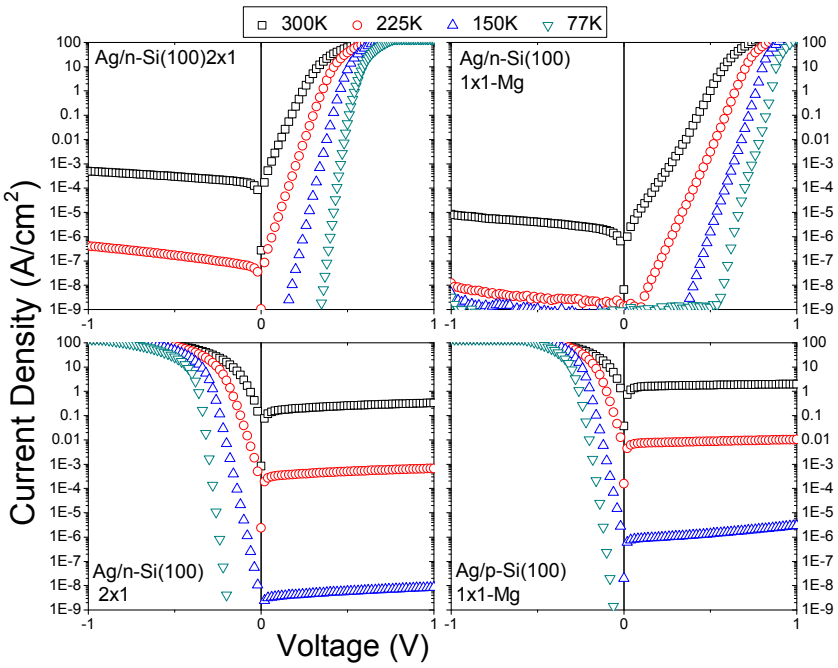

Figure 26. I-V characteristics of Ag on clean 2×1 and Mg-terminated Si (100) 1×1 surfaces at variable temperatures.

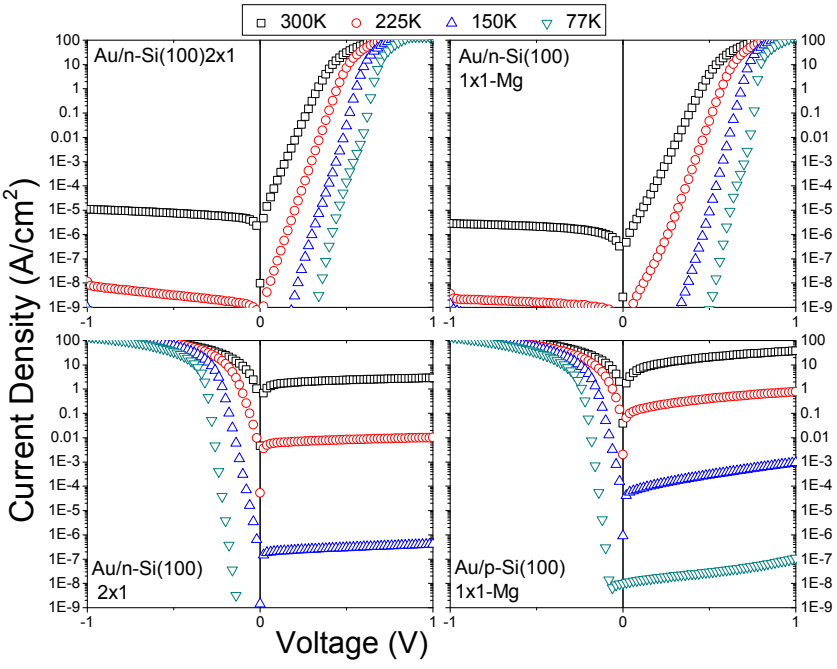

Figure 27. I-V characteristics of Au on clean 2×1 and Mg-terminated Si (100) 1×1 surfaces at variable temperatures.

Ideality factors were consistently observed to be greater than unity. There is also an increase in the ideality factor of the diodes on Mg-terminated surface, compared to that on "clean" surfaces, especially for Au and In. "Leakage component" could also be observed occasionally at low temperature. On Si(111) samples, it was noticeable that current levels at large forward biases (~0.8V-1.0V) were higher at an intermediate temperature of 150K than at any other temperature. This is the consequence of bulk resistivity of Si with 10^{15} doping levels, which has a minimum in the 100-150K temperature range [120].

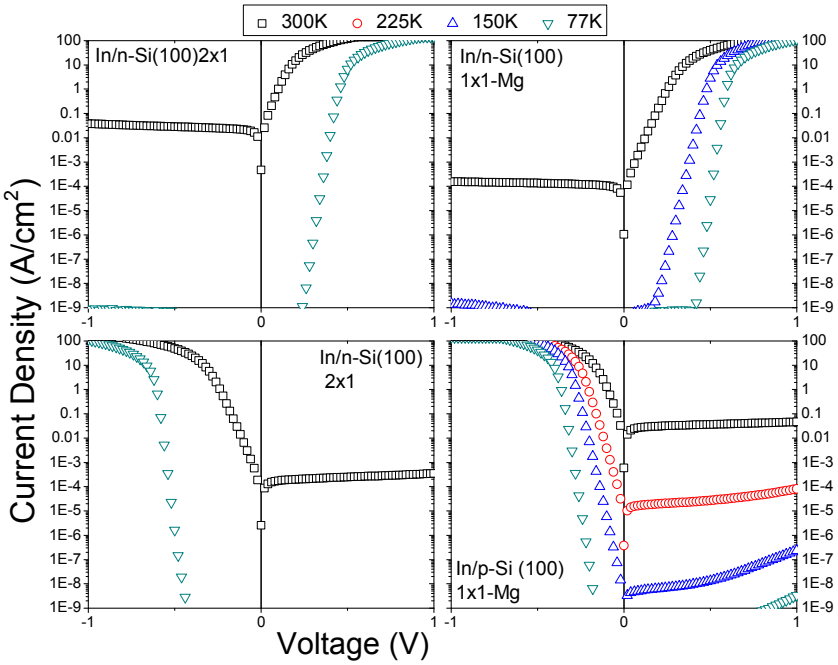

Figure 28. I-V characteristics of In on clean 2×1 and Mg-terminated Si (100) 1×1 surfaces at variable temperatures.

Saturation currents deduced at variable temperatures were also analyzed by Richardson's activation energy plot (See Fig. 29-32) for all interfaces for Ag and Au. Magnitudes of A-E deduced SBH tended to be slightly less than the I-V results. Furthermore, there was a slight curvature in the Richardson's plots, showing that the operative SBH decreased for the lower temperatures.

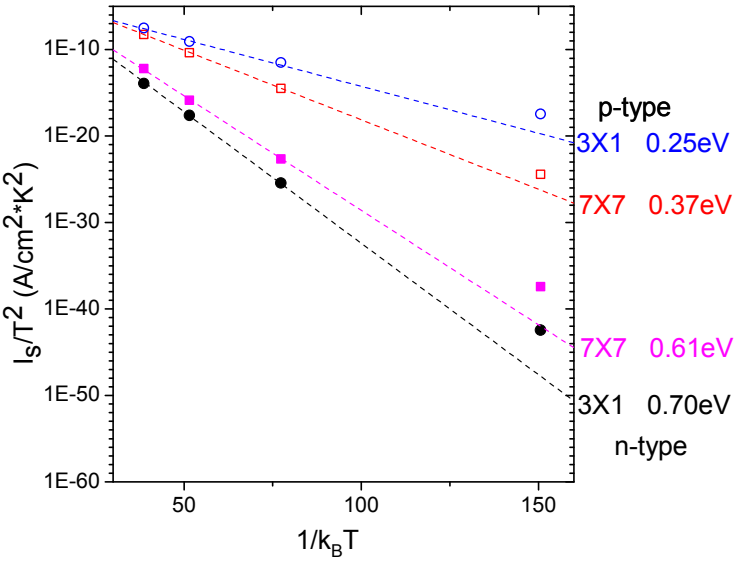

Figure 29. Richardson's A-E plots of Ag on clean Si(111)7×7 and Si(111)3×1-K surfaces.

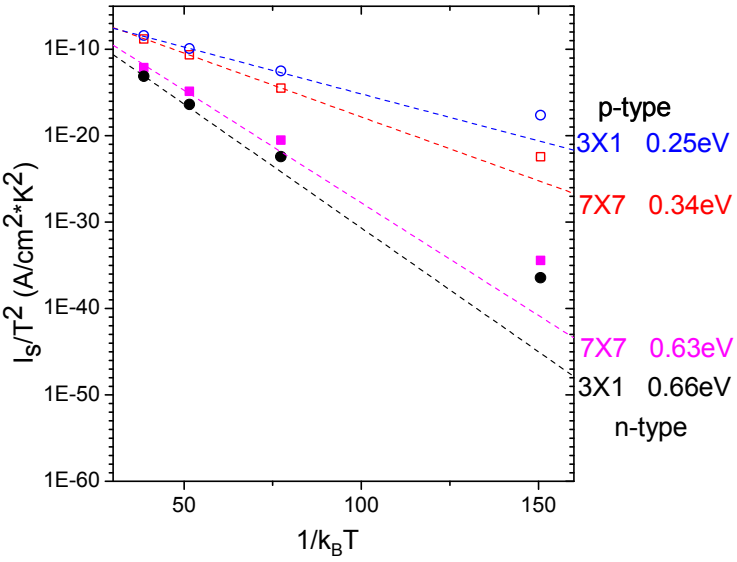

Figure 30. Richardson's A-E plots of Au on clean Si(111)7×7 and Si(111)3×1-K surfaces.

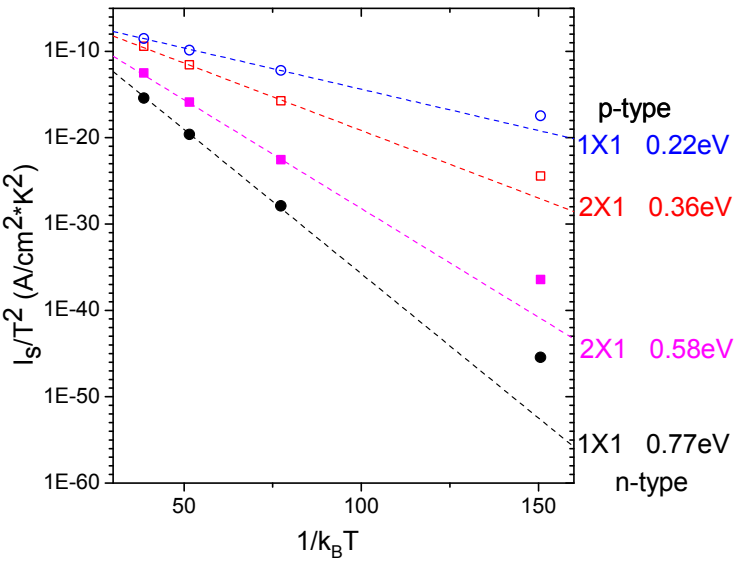

Figure 31. Richardson's A-E plots of Ag on clean Si (100) 2×1 and Si(100)1×1-Mg surfaces.

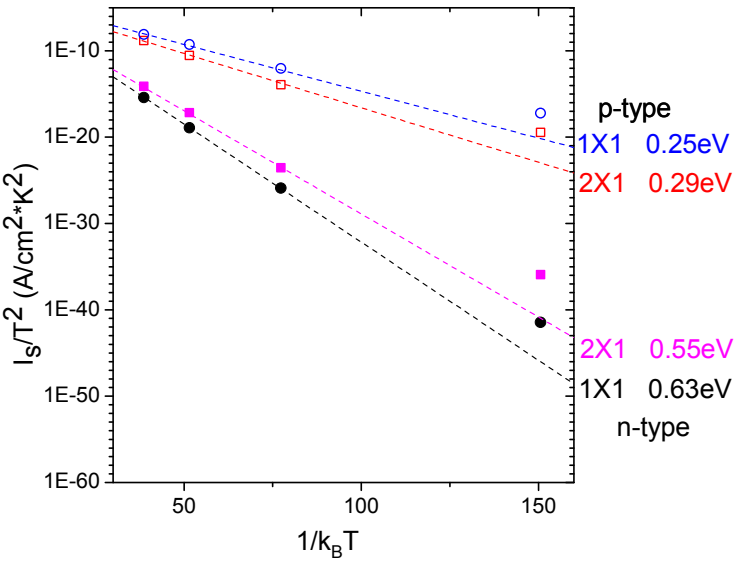

Figure 32. Richardson's A-E plots of Au on clean Si (100) 2×1 and Si(100)1×1-Mg surfaces.

C-V plots in Fig. 33-35 showed the same SBH trends as those seen from I-V and A-E measurements, although SBH values deduced from C-V invariably exceeded I-V results by considerable amounts. Parallel C-V curves in Fig. 33-35 showed nominally no change in the doping level when the surfaces were formed. From all results summarized in Table VI, an SBH shift of 0.10-0.15eV for Si(111)3×1-K and Si(100)1×1-Mg could be concluded for all three metals studied.

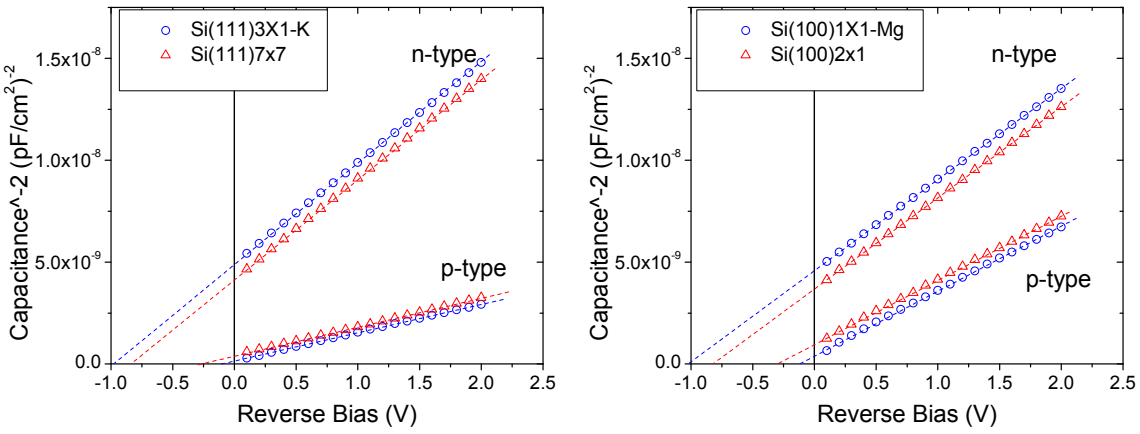

Figure 33. C-V plots of Ag SBH on Si(111)3×1-K and Si(100)1×1-Mg surfaces at 77K and 400 kHz.

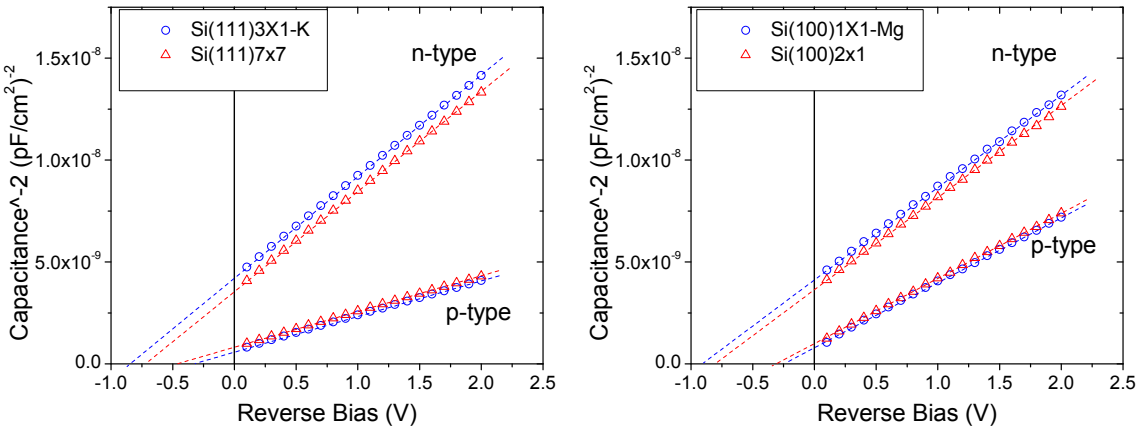

Figure 34. C-V plots of Au SBH on Si(111)3×1-K and Si(100)1×1-Mg surfaces at 77K and 400 kHz.

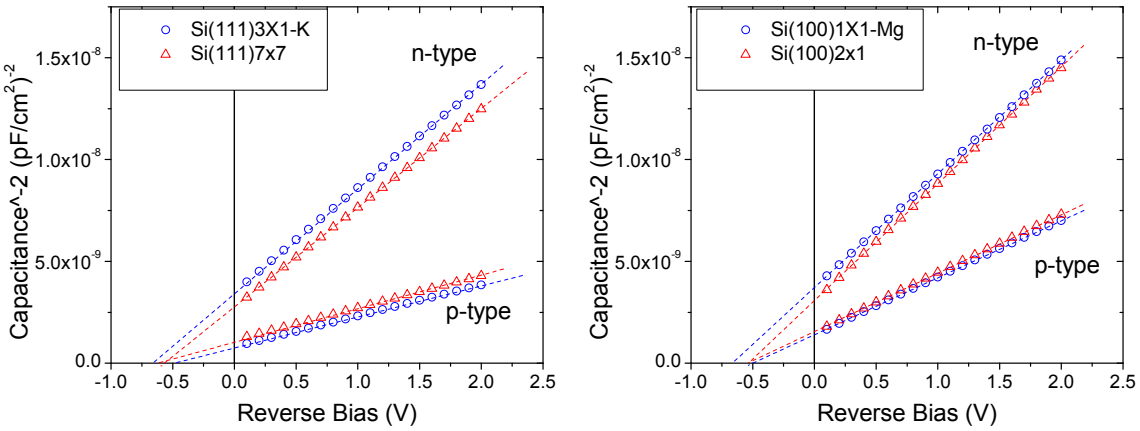

Figure 35. C-V plots of In SBH on Si(111)3×1-K and Si(100)1×1-Mg surfaces at 77K and 400 kHz.

6.2 Discussion

Idealistically, in the absence of any charge rearrangement, the SBH of a metal on an ATS surface is rigorously described by Eq. (25). Presently, the (average) SBHs on Si(111)3×1-K and Si(100)1×1-Mg surfaces were indeed observed to shift in a direction consistent with that of the change in surface EA. However, the magnitude of the SBH shift for K (0.10-0.15eV) was significantly less than KP results (~1.6eV), suggesting that the interaction was quite significant between metal and this ATS. The meta-stability of the Si(111)3×1-K and the large diffusivity of K on Si were previously pointed out [92]. It is plausible that the Si(111)3×1-K surface structure could be significantly compromised upon the deposition of metal. On Si(100)1×1-Mg surface, the observed shifts in the average SBH, ~0.18-0.25 eV for all the metals, from that on the clean Si(100)2×1 was comparable to the change in EA measured for the two free surfaces, ~0.3eV. A plausible interpretation of this observation could be that the higher stability of the Si(100)1×1-Mg surface allowed a significant portion of its surface dipole to be preserved for the MS interface, although the presence of large SBH inhomogeneity at all

Table VI. Summary of measured SBH by I-V, C-V and A-E methods, with deduced ideality factor. Note that all data are presented as a range to demostrate the dominating effect of SBH inhomogeneity.

SBH (eV)			Si(111)		Si(100)	
			clean 7×7	3×1-K	clean 2×1	1×1-Mg
Ag	n-type	I-V	0.65~0.72	0.73~0.79	0.61~0.65	0.78~0.83
		n	1.25~1.03	1.84~1.15	1.33~1.04	1.65~1.20
		A-E	0.58~0.65	0.66~0.71	0.53~0.58	0.69~0.77
		C-V	0.71~0.79	0.81~0.93	0.70~0.74	0.91~0.97
	p-type	I-V	0.34~0.38	0.26~0.30	0.30~0.38	0.20~0.24
		n	1.21~1.06	1.42~1.09	1.20~1.07	1.23~1.10
		A-E	0.32~0.36	0.21~0.26	0.30~0.36	0.19~0.22
		C-V	0.39~0.46	0.30~0.37	0.35~0.43	0.22~0.26
Au	n-type	I-V	0.62~0.74	0.58~0.75	0.55~0.68	0.67~0.74
		n	1.41~1.09	2.03~1.34	1.48~1.19	1.63~1.22
		A-E	0.51~0.63	0.50~0.65	0.50~0.55	0.60~0.63
		C-V	0.72~0.81	0.79~0.90	0.66~0.74	0.82~0.90
	p-type	I-V	0.31~0.36	0.25~0.28	0.28~0.33	0.22~0.29
		n	1.19~1.04	1.43~1.13	1.25~1.06	1.23~1.12
		A-E	0.29~0.34	0.22~0.25	0.25~0.29	0.20~0.25
		C-V	0.35~0.43	0.27~0.36	0.30~0.39	0.23~0.30
In	n-type	I-V	0.48~0.54	0.55~0.61	0.46~0.52	0.63~0.75
		n	1.30~1.12	1.55~1.10	1.33~1.10	1.65~1.23
		C-V	0.58~0.64	0.62~0.75	0.60~0.64	0.77~0.80
	p-type	I-V	0.47~0.50	0.40~0.45	0.50~0.57	0.35~0.41
		n	1.22~1.05	1.33~1.07	1.24~1.03	1.25~1.12
		C-V	0.59~0.61	0.45~0.52	0.59~0.62	0.44~0.50

the MS interfaces clearly indicated that the real interfaces were not as simple as that envisioned by the PI mechanism for perfectly inert ATS surfaces. Presently, clear evidence for inhomogeneous SB's such as non-ideal characteristics, e.g., leakage component in I-V, greater-than-unity ideality factor, lower A-E deduced SBH, curvature in Richardson plots, and the dependence of SBH on techniques of measurement were noted and analyzed by known theories [34, 38] to yield the range of each SBH entry of Table VI. The presence of inhomogeneous SBH for the interfaces presently studied can be attributed to locally varying interface structure. The degrees of observed SBH inhomogeneity (Table VI) tended to be higher on the ATSs than on the

clean Si surfaces, in agreement with the trend observed previously on other ATS surfaces [79, 129]. Likely, with the presence of adsorbate at the MS interface, the range of available structure was considerably widened, leading to the increase in the range of observed SBH. As Table VI reveals, the SBH for any metal appears generally less homogeneous on the Si(111)3×1-K than on the Si(100)1×1-Mg surface, which is consistent with the earlier suggestion that the latter surface appears more stable than the former. Among the three metals studied, Table VI suggests that for a particular surface the SBH of Au is noticeably more inhomogeneous than that deduced for the other two metals. This is not surprising as historically the Au-Si interface has produced an abundance of evidence for significant SBH swings with processing [130-133] although some of these results were attributed to oxygen from the ambient. A higher level of SBH inhomogeneity was also observed for Au in our previous PI studies [79, 129], in fact to the point that perfect ohmic behavior was seen for the Au/n-type Si(100)1×1-S interface!

The FL position for the idealized Si(111)$\sqrt{3}\times\sqrt{3}$-K surface was previously calculated [134] to be located at 0.52 eV above the valance band maximum (VBM), or ~0.11 eV below the FL position measured for the clean Si(111)7×7 surface[118]. As this difference is of the right sign and of comparable magnitude to the observed SBH shift, ~0.10-0.15 eV, it may be tempting to consider an alternative explanation of the present results. One could regard these surface FL positions as charge neutrality levels (CNL) and attribute the presently observed SBH shift to the difference in these CNLs. However, the absolute values of the measured (average) SBH are significantly different from the respective, nominal pinning positions for the free surfaces. Furthermore, the presence of significant SBH inhomogeneity in all the MS interfaces presently investigated suggests that the FL position on the starting surface, while relevant, is not the dominant factor for the SBH. Concerning the Si(100)1×1-Mg, it has been reported that binary

compound magnesium silicide (Mg_2Si) will be formed at Mg-Si interface [100, 135-137] that has the tendency to increase n-type Mg-Si SBH by as much as 0.2eV [136, 137]. For reference, bulk Mg_2Si has an fcc structure with lattice constant a=6.391Å and behaves as a semiconductor with a band gap of 0.7eV [138-140]. It seems that the present SBH shifts on the Si(100)1×1-Mg could be alternatively attributed to Mg silicide formation. As pointed out, the Mg_2Si reaction, when present, is self-limiting at room temperature to ~2ML [100]. At such a thickness and in close proximity to the metal, it is not appropriate to analyze the effect from a stacked layer with the known bulk property of Mg_2Si. Rather, the dipole of the entire MS interface is analyzed as a whole. In the absence of numerical calculations, this analysis essentially reverts to that employed in the PI method. Furthermore, the present surfaces were fabricated under LN2 temperature, and the interface reaction was expected to be significantly reduced.

6.3 Summary

The SBH of Ag, Ag and In on Si(111)3×1-K and Si(100)1×1-Mg surfaces have been studied in detail. Substantial increases in n-type SBH and decreases in p-type SBH, by as much as 0.15eV for K and 0.25V for Mg, were generally deduced from various techniques, in agreement with the expectation of the PI method. Combined with SBH results previously found on As-, Cl-, S- and Ga-terminated surfaces[53, 79, 129], the present work demonstrated a wide range of SBHs on Si accessible with the PI approach, and also shed light on the formation mechanism of the SBH. For the PI method, the present work showed that the chemical stability of the metal-ATS interface was important for the effectiveness of this approach.

CHAPTER 7. SBH Systematics

According to the PI concept, the SBH formed between a metal and an ATS surface is given by Eq. (25) [53]. The adjustability of the SBH is provided by the expected shift of the EA of an ATS surface in a direction that is determined by the electronegativity of the adsorbate relative to Si. Additionally, it is further assumed that for a closed-shell ATS surface with all electrons paired (bonded), the interaction between metal and ATS surface should be small, i.e., the interface dipole term $e\Delta_{IM}$ is small. By terminating all dangling bonds on Si surface by a formation of meta-stable interface layer, in the absence of strong interaction across the interface, the strength of FL pinning is expected to be eliminated or weakened. Without the FL being pinned at the interface, the SBH should vary in a broader range with the choice of metal. It is also the requirement to weaken the strength of the FL pinning that makes the validity and effectiveness of PI technique rely critically on the stability of the ATS surface. The ability of the PI technique in modifying the SBH was systematically studied in this thesis work. ATS surfaces were formed on Si with elements from Groups I-III and V-VII under UHV conditions (expect for Si(111)1×1-Cl surface which was prepared chemically before being introduced into UHV) and were characterized by LEED, AES and KP. Three metals, Ag, Au and In were chosen for SB fabrication, with the magnitude of the SBH being analyzed with the techniques of I-V, C-V and A-E. In addition to detailed interpretation of data, this chapter will focus on the systematic trends demonstrated, e.g., the variation of EA shift with adsorbates, the variation of SBH on a specific ATS surface with metal WF and the variation of SBH on different ATS surfaces with a specific metal, etc. A general conclusion will be drawn, emphasizing the validity and the overall effectiveness of the PI technique.

7.1. Shift in Electron Affinity of ATS Surfaces

In the present work, 7 distinctive ATS surface structures from groups I-III and V-VII, i.e., Si(111)3×1-K, Si(100)1×1-Mg, Si(111)$\sqrt{3}\times\sqrt{3}$ -Ga, Si(111)6.3×6.3- Ga, Si(111)1×1-As, Si(100)1×1-S, and Si(111)1×1-Cl. The EA for all of these surfaces were measured by KP with respect to the corresponding clean Si surface. As summarized in Table VII, the average of measured n-type and p-type shifts in WF ($\Delta\phi = \phi_{ATS} - \phi_{clean}$), in the absence of information on the surface FL position, was suggestive of a shift in the EA ($\Delta\phi = \phi_{ATS} - \phi_{clean}$) of the same magnitude. Experimental or theoretical EA values from the literature, where available, are also listed for comparison. Note that the Si(111)1×1-H surface, which was formed prior to the chlorination process, is also included as a reference to show the effect of Cl-termination. Since Si(111)1×1-H surface is not expected to survive any metal deposition, those results cannot be viewed as meaningful for comparison.

For Si(111)1×1-As, Si(100)1×1-S, Si(111)$\sqrt{3}\times\sqrt{3}$ -Ga, Si(111)6.3×6.3-Ga, Si(111)3×1-K and Si(100)1×1-Mg surfaces, quite similar WF shifts for both n-type and p-type were obtained. Generally, results on heavily doped n-type substrates may be more preferable to those on lightly doped p-type substrates. The small discrepancy between n-type and p-type value may be attributed to surface contaminations and inevitably involved human errors, e.g. distance from the tip to the sample and/or lateral position of the tip. The EA shifts on Si(111)1×1-As surface was in good agreement with the available reference, while EA shift on Si(100)1×1-S surface was significantly less. Interestingly, the results obtained on Si(111)1×1-Cl n-type surface differed by ~0.4eV from that measured on p-type surface with the same surface structure, although the average of these two values agreed closely with the theoretical prediction [53, 119]. In the

present thesis work, EA shifts Si(111)$\sqrt{3}\times\sqrt{3}$-Ga, Si(111)6.3×6.3-Ga, Si(100)1×1-Mg and Si(111)3×1-K were found to be -0.23eV, -0.27eV, -0.33eV and -1.62eV, respectively. The WF or AE shifts obtained on Si(111)$\sqrt{3}\times\sqrt{3}$-Ga and Si(111)6.3×6.3-Ga surfaces were close, though slightly smaller than that suggested [119]. This similarity is expected according to the surface geometries of these surfaces. For Si(111)$\sqrt{3}\times\sqrt{3}$-Ga surface, theoretical calculations showed that Ga atoms are located 1.35Å above the Si plane [84], while on Si(111)6.3×6.3-Ga surface this number is roughly the spacing between Si double plane, 0.5Å [126]. On the other hand, surface coverage for Si(111)6.3×6.3-Ga surface is 3 times of that on Si(111)$\sqrt{3}\times\sqrt{3}$-Ga surface (1ML vs. 1/3ML). In a simple view of surface dipole formation, the combination of charge density and spatial distance gives roughly equal surface dipoles that are suggestive reasonably similar EA shifts.

Table VII. Change in work function/electron affinity of ATS surfaces.

Shift in WF or EA (eV)	$\Delta\phi$ (n-type)	$\Delta\phi$ (p-type)	$\Delta\chi$ (expt.)	$\Delta\chi$ (ref.)
Si(111)1×1-Cl	+0.61	+1.05	(+0.83)	+0.82
Si(100)1×1-S	+0.14	+0.12	(+0.13)	+0.45
Si(111)1×1-As	+0.27	+0.33	(+0.30)	+0.40
Si(111)$\sqrt{3}\times\sqrt{3}$-Ga	-0.26	-0.20	(-0.23)	-0.40
Si(111)6.3×6.3-Ga	-0.33	-0.22	(-0.27)	-
Si(100)1×1-Mg	-0.32	-0.35	(-0.33)	-
Si(111)3×1-K	-1.66	-1.58	(-1.62)	(-1.4)
Si(111)1×1-H	-0.28	+0.12	(-0.07)	-0.21

The general trend of EA shift can be thus concluded as follows: for elements from groups V-VII, the measured EA's were consistently greater than that on clean Si. This is in agreement of the suggested increase EA due to negative interface dipole (surface negative, bulk positive) originated from the expected charge transfer from Si to elements with larger electronegativities. On the other hand, for ATS formed with group I-III elements, EA's were consistently less, in agreement with the adsorbate-to-Si charge transfer and resultant positive (surface positive, bulk negative) surface dipole.

7.2. Shift in Schottky Barrier Height

Upon formation of the above ATS surfaces, Schottky diodes were fabricated with the chosen metals, Au, Ag and In. The magnitudes of the SBH's obtained by means of I-V, C-V and A-E were reported with the existence of non-ideal behaviors, e.g., apparent leakage components, greater-than-unity ideality factors, low-slope A-E tail-offs, small active conducting areas, dependence of SBH on measurement technique, etc, which have been shown as natural consequence of inhomogeneous SB's. As being dominated by large degrees of inhomogeneity, the values of SBH's were presented in significant ranges, with information on the non-uniformity at the interface being indicated. A lower bound of I-V or A-E measured value may be governed by the current transport through low-SBH regions at low temperatures, higher values of I-V and/or A-E results should be treated as nominal values to be included to demonstrate the shift in SBH. While C-V is relatively less sensitive to the details of the interface, or the inhomogeneity, an average of the slightly scattered results may be adequately used in the current analysis. Measured shift in SBH on ATS surfaces with respect to that on clean surfaces are summarized in Table VIII and Table IX.

Table VIII. Change in SBH (eV) on ATS surfaces, from I-V measurements.

Shift in SBH (eV)	Ag		Au		In	
	n-type	p-type	n-type	p-type	n-type	p-type
Si(111)1×1-Cl	-0.19	+0.26	-0.29	+0.12	-0.48	+0.05
Si(100)1×1-S	-0.17	+0.18	-0.56	+0.06	-0.09	+0.14
Si(111)1×1-As	-0.34	+0.25	-0.04	+0.08	-0.50	+0.20
Si(111)$\sqrt{3}\times\sqrt{3}$-Ga	+0.11	-0.12	+0.05	-0.13	+0.06	-0.12
Si(111)6.3×6.3-Ga	+0.14	-0.14	+0.07	-0.15	+0.11	-0.11
Si(100)1×1-Mg	+0.17	-0.14	+0.06	-0.04	+0.19	-0.11
Si(111)3×1-K	+0.07	-0.08	+0.01	-0.08	+0.07	-0.05

As revealed by Table VIII, I-V measurements showed that for all three metals, the n-type SBH's on As-, Cl- and S-terminated Si surfaces were lowered by as much as 0.5eV, 0.48eV and 0.17eV, respectively, while p-type SBH increased by 0.25eV, 0.26 and 0.18eV. It should be noted that the huge drop (0.56eV) in n-type SBH of Au on the Si(100)1×1-S has been attributed to the presence of a small number of low-SBH (~0.03eV) regions that rendered the I-V behavior of the entire diode perfectly "ohmic". In contrast, for SBH's on Ga-, K- and Mg-terminated Si surface, a direct opposite was observed, where increased n-type SBH's of 0.15eV, 0.10eV and 0.20eV, respectively, were obtained and p-type SBH decreased by 0.15eV, 0.08eV and 0.14eV respectively. The systematic trend in the SBH shifts deduced from I-V data could be accounted for by the trend in EA, as suggested by the PI method. A change in EA will result in a shift in SBH by the same amount, provided that the metal-ATS interaction is small. Therefore, a simple comparison of the actual SBH shift with the change in EA may reveal information on the stability of ATS surface. For instance, KP measurement suggested a 1.6eV drop in EA for the

Si(111)3×1-K surface, implying an increase in the n-type SBH by 1.6eV within the idealistic picture. Under no circumstances will this ever be possible, because the Si band gap is only 1.12 eV and the FL has to reside inside the band gap for charge neutrality. In cases like this, a charge transfer has to take place between the metal and the ATS, i.e. the metal and the ATS have to interact, to bring the FL inside the band gap. From the perspective of chemistry, this represents a driving force for the interface structure to change. Therefore, the actually-measured 0.14eV increase in n-type SBH for the Si(111)3×1-K interface is evidence for metal-ATS interaction, which likely involves a disruption of the original ATS structure.

Table IX. Change in SBH on ATS surfaces, from C-V measurements.

Shift in SBH (eV)	Ag		Au		In	
	n-type	p-type	n-type	p-type	n-type	p-type
Si(111)1×1-Cl	-0.22	+0.37	-0.49	+0.60	-0.50	+0.05
Si(100)1×1-S	-0.19	+0.23	-0.56(IV)	+0.19	-0.12	+0.14
Si(111)1×1-As	-0.40	+0.27	-0.09	+0.48	-0.48	+0.20
Si(111)$\sqrt{3}\times\sqrt{3}$-Ga	+0.15	-0.11	+0.11	-0.08	+0.15	-0.08
Si(111)6.3×6.3-Ga	+0.17	-0.17	+0.12	-0.08	+0.14	-0.05
Si(100)1×1-Mg	+0.25	-0.07	+0.16	-0.12	+0.16	-0.12
Si(111)3×1-K	+0.14	-0.09	+0.09	-0.07	+0.11	-0.09

SBH shifts deduced from CV data, as shown in Figure IX, demonstrated a similar trend with that by I-V, although with some reasonable discrepancies in magnitude. Following the logic that C-V results are more preferable for SBH shift study, based on the nature of insensitivity to

inhomogeneous SBH, the C-V data should be more suitable for the analysis of the weakening of metal-semiconductor interactions.

7.3. Weakening of Metal-Semiconductor Interactions

The SBH is a property of the interface between a metal and a semiconductor, and naturally depends on the properties of both. If the expected SBH dependencies on the metal and the semiconductor were put on more equal footings, one can express the SBH as an expansion

$$d\Phi_{Bn} = \left.\frac{\partial \Phi_{Bn}}{\partial \varphi_M}\right|_{SC} d\varphi_M + \left.\frac{\partial \Phi_{Bn}}{\partial \chi_{SC}}\right|_{M} d\chi_{SC} \equiv S_{SC} d\varphi_M - S_M d\chi_{SC}, \tag{26}$$

for small departures from a particular metal-semiconductor (M-SC) pair. In the above, S_{SC} is the familiar interface behavior parameter, defined in Eq. (3). That this should be a property of the semiconductor surface is clear, on account that the semiconductor surface is the only "constant" in such a systematic study. It follows then that the S-parameter of the metal in Eq. (26), defined as

$$-\left.\frac{\partial \Phi_{Bn}}{\partial \chi_{SC}}\right|_{M} = S_M, \tag{27}$$

describes how "reactive" or "interactive" a metal is. We should note that the present MS interfaces represent a very unusual class of material interfaces in SBH studies: the EA of the present semiconductor surfaces can be varied, while keeping the band gap of the semiconductor constant. Ordinarily, with a change in the semiconductor EA, e.g. from Si to GaAs, the band gap changes inevitably. Under ordinary conditions, a study of the metallic interface behavior makes little sense, due to the dominant contribution associated with the change in the bulk band

structure. The unusual circumstances of the present MS interfaces allow both types of analysis, S_M and S_{SC}, to be made, with different perspectives on the MS interaction.

It has been mentioned earlier that any effective method to modify the SBH must have a strategy to overcome or weaken the MS interactions, sometimes referred as FL pinning phenomenon. The PI technique assumes weak metal-ATS interactions on ATS surfaces, as Eq. (25). Therefore, to verify the effect of weakening the MS interactions by the PI mechanism, one may study the dependence of SBH on either metal WF or EA of ATS. Since the CNL positions for Ag, Au and In on those ATS surfaces are largely unknown, we can estimate the strength of metal-ATS interactions (or the strength of FL pinning) thought their electrical properties. By plotting SBH versus metal WF (study of S_{SC} parameter) and SBH shift versus EA shift of ATS for a specific metal (study of S_M parameter), the FL condition and stability of ATS surface are expected to be illustrated.

Previously, the dependence of n-type SBH on metal WF obtained on Si(111)1×1-As, Si(100)1×1-S and Si(111)1×1-Cl surfaces were analyzed [79]. Among these surfaces, the Si(111)1x1-As was the one on which the SBH was observed to increase most readily with the metal WF. An S_{SC} parameter of 0.53 was deduced for the Si(111)1×1-As surface, compared to 0.12 on clean Si(111)7×7 surface, which suggested that the Si(111)1×1-As surface is more chemically stable than Si(100)1×1-S and Si(111)1×1-Cl surfaces. For those surfaces, such consistency was observed for Ag and In SBH's, except for Au SBH's. The lower values of Au SBH observations were likely due to more significant interactions between Au and these ATS surfaces and large degree of SBH inhomogeneity [79], in comparison with those for Ag and In.

Same analysis was applied to Ag, Au and In on Si(111)$\sqrt{3}\times\sqrt{3}$ -Ga, Si(111)6.3×6.3-Ga, Si(100)1×1-Mg and Si(111)3×1-K surfaces, as shown in Fig. 36. Despite Au results, a consistent increase in n-type Ag and In SBH's with metal WF on these surfaces is demonstrated and an elevated S_M parameter can be deduced (black dotted line vs. pink dotted line), suggesting weakening of MS interactions by ATS surfaces. However, evidences of metal-ATS interactions for Au SBH were clearly demonstrated, in a manner quite similar to that on Si(100)1×1-S and Si(111)1×1-Cl surfaces, likely due to strong interactions between Au and ATS surfaces.

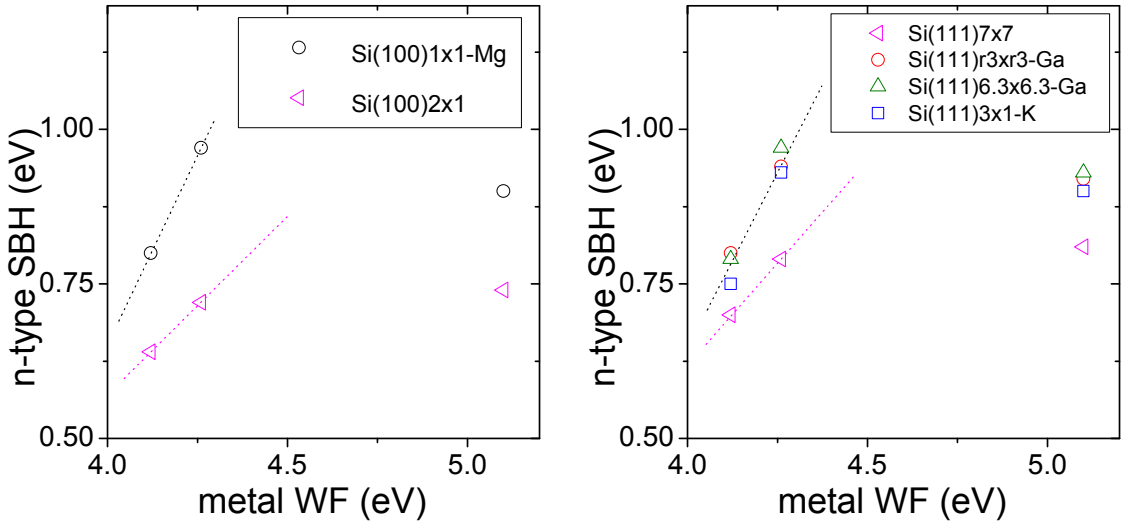

Figure 36. Dependence of n-type SBH's on various surfaces on metal WF (In, 4.12 eV; Ag, 4.26 eV; and Au, 5.1 eV).

A plot of the SBH shifts against the EA shifts of a metal on different ATS surfaces (Fig. 37) is an approach to study the S_M parameter. The extent of MS interaction decreases as this quantity goes from 0 to 1. Note that results on Si (111) and Si (100) are plotted on the same graph due to the similar values of SBH on clean surfaces, which is treated as a constant. Thus the slope on the graph for each metal, $-d\left(\Phi_{B,n}-\Phi_{B,n}^{clean}\right)/d\chi_{ATS}$, is equivalent to S_M. From the

graph one can see that Ag (S_M =0.90) has the least interactions with those ATS surfaces, while In (S_M =0.66) and Au (S_M =0.38) interact more with the interface. This is in agreement with the electronegativities of those metals in comparison with that of Si. Ag has an electronegativity of 1.93, which is very close to that of Si (1.90), while electronegativities for Au and In are 2.4 and 1.78, respectively. From the perspective of chemical reaction, Ag should have a smaller driving force to interact with Si than the other metals, and therefore is more likely to keep the surface structure intact. This is also consistent with the deduction from electrical measurements that Ag-ATS surfaces are more uniform than either the Au-ATS or the In-ATS. Furthermore, it seems that the 3 fitted lines roughly intersect at one point. This is expected and the intersection should be the origin, in principle. However, uncertainties of SBH measurement could possibly be responsible for any deviation from the origin. It is to be reminded that K- and Cl-terminated surfaces are not included in this argument because of the strong FL pinning that confines the FL in the Si band-gap with a significant shift in EA.

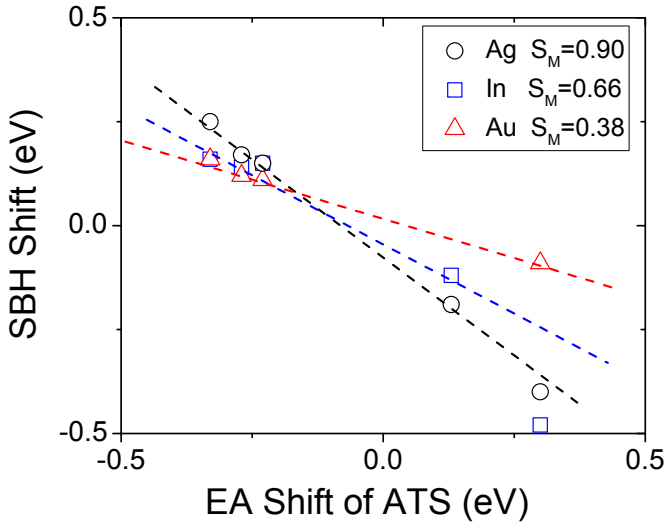

Figure 37. Dependence of SBH shift on EA shift of ATS surfaces.

7.4. Conclusion

A systematic modification of the SBH was demonstrated through the proposed partisan interlayer (PI) method. SBH was dramatically tuned, in the intended direction, by changing the atomic structure and the EA of the starting semiconductor surface. The SBH of Ag, Ag and In on surfaces terminated by elements with electronegativity smaller than that of silicon have been studied in detail. Substantial increases in n-type SBH and decreases in p-type SBH, were generally deduced from various techniques, in agreement with the expectation of the PI method. Combined with SBH results previously found on As-, Cl- and S-terminated surfaces[53, 79], the present work demonstrated a wide range of SBHs on Si accessible with the PI approach, and also shed light on the formation mechanism of the SBH. However, all interfaces presently investigated, including those on Ga-terminated and clean Si surfaces, were found to be inhomogeneous. This is a very common feature of most non-epitaxial MS interfaces [4, 34, 127, 128], and is an issue that needs to be dealt with in the development of SBH tuning technologies. For the PI method, the present work showed that the chemical stability of the metal-ATS interface was important for the effectiveness of this approach. The effect of the SBH modification by partisan interlayer is predictable, simply from the electronegativity consideration and the chemical stability of the adsorbate-terminated surfaces against metal interaction. A systematic method to vary the SBH thus emerged and seemed viable for advanced applications.

REFERENCES

1. Tung, R.T., *Recent advances in Schottky barrier concepts.* Materials Science and Engineering: R: Reports, 2001. **35**(1-3).
2. Brillson, L.J., *Surfaces and Interfaces of Electronic Materials*. 1st ed. 2010, Berlin: Wiley-VCH.
3. Heslinga, D.R., et al., *Atomic-structure-dependent Schottky barrier at epitaxial Pb/Si(111) interfaces.* Physical Review Letters, 1990. **64**(13): p. 1589-1592.
4. Tung, R.T., *Schottky-Barrier formation at single-crystal metal-semiconductor interfaces.* Physical Review Letters, 1984. **52**(6): p. 461-464.
5. Wang, A. and W.A. Anderson, *Metal-semiconductor contacts to n-ZnS 0.07Se 0.93.* Journal of Electronic Materials, 1996. **25**(2): p. 201-205.
6. Hasegawa, F., et al., *Reduction of Schottky barrier heights by surface oxidation of GaAs and its influence on DLTS signals for the midgap level EL2.* Solid State Electronics, 1988. **31**(2): p. 223-228.
7. Hattori, K. and Y. Torii, *A new method to fabricate Au/n-type InP Schottky contacts with an interfacial layer.* Solid-State Electronics, 1991. **34**(5): p. 527-531.
8. Coleman, J.J., *Controlled barrier height InP Schottky diodes prepared by sulfur diffusion.* Applied Physics Letters, 1977. **31**(4): p. 283-285.
9. Song, G., M.Y. Ali, and M. Tao, *A high Schottky barrier between Ni and S-passivated n-type Si(1 0 0) surface.* Solid-State Electronics, 2008. **52**(11): p. 1778-1781.
10. Tung, R.T., *Chemical bonding and fermi level pinning at metal-semiconductor interfaces.* Physical Review Letters, 2000. **84**(26): p. 6078-6081.
11. Tung, R.T., *Formation of an electric dipole at metal-semiconductor interfaces.* Physical Review B - Condensed Matter and Materials Physics, 2001. **64**(20): p. 2053101-20531015.
12. Sze, S.M. and K.K. Ng, *Physics of Semiconductor Devices*. 3 ed. 2007, Hoboken, New Jersey: John Wiley & Sons, Inc.
13. Mott, N.F., *The theory of crystal rectifiers.* Proceedings of the Royal Society of London Series a-Mathematical and Physical Sciences, 1939. **171**(A944): p. 0027-0038.
14. Schottky, W., *Halbleitertheorie der Sperrschicht.* Die Naturwissenschaften, 1938. **26**(52): p. 843.
15. Schlüter, M., *Chemical trends in metal-semiconductor barrier heights.* Physical Review B, 1978. **17**(12): p. 5044-5047.
16. Mead, C.A. and W.G. Spitzer, *Fermi Level Position at Metal-Semiconductor Interfaces.* Physical Review, 1964. **134**(3A): p. A713.
17. Bardeen, J., *Surface states and rectification at a metal semi-conductor contact.* Physical Review, 1947. **71**(10): p. 717-727.
18. Cowley, A.M. and S.M. Sze, *Surface states and barrier height of metal-semiconductor systems.* Journal of Applied Physics, 1965. **36**(10): p. 3212-3220.
19. Louie, S.G. and M.L. Cohen, *Electronic structure of a metal-semiconductor interface.* Physical Review B, 1976. **13**(6): p. 2461-2469.
20. Mönch, W., *Barrier heights of real Schottky contacts explained by metal-induced gap states and lateral inhomogeneities.* Journal of Vacuum Science and Technology B: Microelectronics and Nanometer Structures, 1999. **17**(4): p. 1867-1876.

21. Tersoff, J., *Schottky barriers and semiconductor band structures.* Physical Review B, 1985. **32**(10): p. 6968-6971.
22. Heine, V., *Theory of surface states.* Physical Review, 1965. **138**(6A): p. A1689-A1696.
23. Spicer, W.E., et al., *Unified defect model and beyond.* Journal of Vacuum Science and Technology, 1980. **17**(5): p. 1019.
24. Fujitani, H. and S. Asano, *Schottky barriers at NiSi2/Si(111) interfaces.* Physical Review B, 1990. **42**(3): p. 1696-1704.
25. Van Schilfgaarde, M. and N. Newman, *Electronic structure of ideal metal/GaAs contacts.* Physical Review Letters, 1990. **65**(21): p. 2728-2731.
26. Dandrea, R.G. and C.B. Duke, *Calculation of InAs/AlSb(001) band offsets: Effect of strain and interfacial atomic structure.* Applied Physics Letters, 1993. **63**(13): p. 1795-1797.
27. Rhoderick, E.H. and R.H. Williams, *Metal-Semiconductor Contacts*. 2 ed. 1988, New York: Oxford University Press, USA.
28. Bethe, H.A., *Theory of Boundary Layer of Crystal Rectifiers.* MIT Radiaon Laboratory Report, 1942(43): p. 12.
29. Crowell, C.R. and S.M. Sze, *Current transport in metal-semiconductor barriers.* Solid State Electronics, 1966. **9**(11-12): p. 1035-1048.
30. Berz, F., *The Bethe condition for thermionic emission near an absorbing boundary.* Solid State Electronics, 1985. **28**(10): p. 1007-1013.
31. Baccarani, G., *Current transport in Schottky-barrier diodes.* Journal Of Applied Physics, 1976. **47**(9): p. 4122-4126.
32. Chang, C.Y. and S.M. Sze, *Carrier transport across metal-semiconductor barriers.* Solid-state Electronics, 1970. **13**(6): p. 727-740.
33. Andrews, J.M. and M.P. Lepselter, *Reverse current-voltage characteristics of metal-silicide Schottky diodes.* Solid-state Electronics, 1970. **13**(7): p. 1011-1023.
34. Tung, R.T., *Electron transport at metal-semiconductor interfaces: General theory.* Physical Review B, 1992. **45**(23): p. 13509-13523.
35. Hauenstein, R.J., et al., *Schottky barrier height measurements of epitaxial NiSi2 on Si.* Applied Physics Letters, 1985. **47**(8): p. 853-855.
36. Tung, R.T., *Schottky Barrier Heights of Single Crystal Silicides on Si(111).* Journal of Vacuum Science and Technology B: Microelectronics and Nanometer Structures, 1984. **2**(3): p. 465-470.
37. Das, G.P., et al., *Electronic structure and Schottky-barrier heights of (111) NiSi2/Si A- and B-type interfaces.* Physical Review Letters, 1989. **63**(11): p. 1168-1171.
38. Tung, R.T., *Electron transport of inhomogeneous Schottky barriers.* Applied Physics Letters, 1991. **58**(24): p. 2821.
39. Ohdomari, I., T.S. Kuan, and K.N. Tu, *Microstructure and Schottky barrier height of iridium silicides formed on silicon.* Journal Of Applied Physics, 1979. **50**(11): p. 7020-7029.
40. Canali, C., et al., *Thin Pt and Pd silicide Schottky barriers for silicon solar cells.* Journal of Physics D: Applied Physics, 1977. **10**(18): p. 2481-2489.
41. Ohdomari, I. and K.N. Tu, *Parallel silicide contacts.* Journal Of Applied Physics, 1980. **51**(7): p. 3735-3739.
42. Freeouf, J.L., et al., *Size Dependence of "Effective" Barrier Heights of Mixed-Phase Contacts.* Journal of Vacuum Science and Technology, 1982. **V 21**(N 2): p. 570-573.

43. Freeouf, J.L., et al., *Effective barrier heights of mixed phase contacts: Size effects.* Applied Physics Letters, 1982. **40**(7): p. 634-636.
44. Werner, J.H., *Schottky barrier and pn-junction I/V plots - Small signal evaluation.* Applied Physics A Solids and Surfaces, 1988. **47**(3): p. 291-300.
45. Padovani, F.A. and G.G. Sumner, *Experimental study of gold-gallium arsenide Schottky barriers.* Journal Of Applied Physics, 1965. **36**(12): p. 3744-3747.
46. Saxena, A.N., *Forward current-voltage characteristics of Schottky barriers on n-type silicon.* Surface Science, 1969. **13**(1): p. 151-171.
47. Tuck, B., G. Eftekhari, and D.M. De Cogan, *The Al-(n-InP) Schottky barrier.* Journal of Physics D: Applied Physics, 1982. **15**(3): p. 457-465.
48. Yu, A.Y.C. and E.H. Snow, *Surface effects on metal-silicon contacts.* Journal Of Applied Physics, 1968. **39**(7): p. 3008-3016.
49. Chin, V.W.L., J.W.V. Storey, and M.A. Green, *Characteristics of p-type PtSi Schottky diodes under reverse bias.* Journal Of Applied Physics, 1990. **68**(8): p. 4127-4132.
50. Newman, N., et al., *Electrical study of Schottky barriers on atomically clean GaAs(110) surfaces.* Physical Review B, 1986. **33**(2): p. 1146-1159.
51. Thanailakis, A. and A. Rasul, *Transition-metal contacts to atomically clean silicon.* Journal of Physics C: Solid State Physics, 1976. **9**(2): p. 337-343.
52. Hökelek, E. and G.Y. Robinson, *A comparison of Pd Schottky contacts on InP, GaAs and Si.* Solid State Electronics, 1981. **24**(2): p. 99-103.
53. Li, Y., W. Long, and R.T. Tung, *Controlled modification of Schottky barrier height by partisan interlayer.* Solid State Communications, 2011. **151**(22): p. 1641-1644.
54. Campbell, I.H., et al., *Controlling Schottky energy barriers in organic electronic devices using self-assembled monolayers.* Physical Review B - Condensed Matter and Materials Physics, 1996. **54**(20): p. R14321-R14324.
55. Haick, H., et al., *Controlling semiconductor/metal junction barriers by incomplete, nonideal molecular monolayers.* Journal of the American Chemical Society, 2006. **128**(21): p. 6854-6869.
56. Haick, H., et al., *Controlling Au/n-GaAs junctions by partial molecular monolayers.* Physica Status Solidi (A) Applications and Materials Science, 2006. **203**(14): p. 3438-3451.
57. Hsu, J.W.P., et al., *Nature of electrical contacts in a metal-molecule-semiconductor system.* Journal of Vacuum Science and Technology B: Microelectronics and Nanometer Structures, 2003. **21**(4): p. 1928-1935.
58. Kampen, T., et al., *Barrier heights of organic modified Schottky contacts: Theory and experiment.* Applied Surface Science, 2004. **234**(1-4): p. 313-320.
59. Lodha, S., P. Carpenter, and D.B. Janes, *Effect of contact properties on current transport in metal/molecule/GaAs devices.* Journal of Applied Physics, 2006. **99**(2): p. 1-9.
60. Selzer, Y. and D. Cahen, *Fine tuning of Au/SiO2/Si diodes by varying interfacial dipoles using molecular monolayers.* Advanced Materials, 2001. **13**(7): p. 508-511.
61. Vilan, A., A. Shanzer, and D. Cahen, *Molecular control over Au/GaAs diodes.* Nature, 2000. **404**(6774): p. 166-168.
62. Wang, W., T. Lee, and M.A. Reed, *Mechanism of electron conduction in self-assembled alkanethiol monolayer devices.* Physical Review B - Condensed Matter and Materials Physics, 2003. **68**(3): p. 354161-354167.

63. Zuppiroli, L., et al., *Self-assembled monolayers as interfaces for organic opto-electronic devices.* European Physical Journal B, 1999. **11**(3): p. 505-512.
64. Becker, R.S., et al., *Geometric and Local Electronic Structure of Si(111)-As.* Physical Review Letters, 1988. **60**(2): p. 116.
65. Copel, M. and R.M. Tromp, *Structural perfection of the Si(111)-(1×1) As surface.* Physical Review B, 1988. **37**(5): p. 2766.
66. Copel, M., et al., *Atomic structure of the arsenic-saturated Si(111) surface.* Physical Review B, 1988. **37**(18): p. 10756.
67. Headrick, R.L. and W.R. Graham, *Geometric structure of the Si(111): As-1×1 surface.* Physical Review B, 1988. **37**(2): p. 1051.
68. Hybertsen, M.S. and S.G. Louie, *Theory of quasiparticle surface states in semiconductor surfaces.* Physical Review B, 1988. **38**(6): p. 4033.
69. Olmstead, M.A., et al., *Arsenic overlayer on Si(111): Removal of surface reconstruction.* Physical Review B, 1986. **34**(8): p. 6041.
70. Uhrberg, R.I.G., et al., *Electronic structure, atomic structure, and the passivated nature of the arsenic-terminated Si(111) surface.* Physical Review B, 1987. **35**(8): p. 3945.
71. Uhrberg, R.I.G. and G.V. Hansson, *Electronic structure of silicon surfaces. Clean and with ordered overlayers.* Critical Reviews in Solid State and Materials Sciences, 1991. **17**(2): p. 133-186.
72. Boland, J.J. and J.S. Villarrubia, *Formation of Si(111)-(1×1)Cl.* Physical Review B, 1990. **41**(14): p. 9865.
73. Eves, B.J. and G.P. Lopinski, *Formation and reactivity of high quality halogen terminated Si(1 1 1) surfaces.* Surface Science, 2005. **579**(2-3): p. L89.
74. Rivillon, S., et al., *Gas phase chlorination of hydrogen-passivated silicon surfaces.* Applied Physics Letters, 2004. **85**: p. 2583.
75. Sakurai, S. and T. Nakayama, *Cl adsorption process on Si(1 1 1) surfaces.* Surface Science, 2001. **493**(1-3): p. 143-147.
76. Lacharme, J.P., N. Benazzi, and C.A. Sebenne, *Compositional and electronic properties of Si(001)2×1 upon diatomic sulfur interaction.* Surface Science, 1999. **433-435**: p. 415-419.
77. Kaxiras, E., *Semiconductor-surface restoration by valence-mending adsorbates: Application to Si(100):S and Si(100):Se.* Physical Review B, 1991. **43**(8): p. 6824-6827.
78. Li, Y., *PhD Dissertation.* 2012.
79. Li, Y., W. Long, and R.T. Tung, to be published.
80. Ishizaka, A. and Y. Shiraki, *Low Temperature Surface Cleaning of Silicon and Its Application to Silicon MBE.* Journal of the Electrochemical Society, 1986. **133**(4): p. 666-671.
81. Jousten, K., *Wutz Handbuch Vakuumtechnik*. 10 ed. 2009, Frider. Vieweg & Sohn Verlag: Wiesbaden.
82. Zegenhagen, J., et al., *Monolayer growth and structure of ga on si(111).* Physical Review B, 1988. **38**(11): p. 7885-7888.
83. Zegenhagen, J., et al., *Discommensurate Reconstructions of (111)Si and Ge Induced by Surface Alloying with Cu, Ga and In.* Physica Status Solidi (B) Basic Research, 1997. **204**(2): p. 587-616.
84. Kawazu, A. and H. Sakama, *Geometric structure of the Si(111)Š3×Š3-Ga surface.* Physical Review B, 1988. **37**(5): p. 2704-2706.

85. Lai, M.Y. and Y.L. Wang, *Gallium-induced nanostructures on Si(111): From magic clusters to incommensurate structures.* Physical Review B - Condensed Matter and Materials Physics, 1999. **60**(3): p. 1764-1770.
86. Čechal, J., et al., *Gallium structure on the Si(111)-(7 × 7) surface: Influence of Ga coverage and temperature.* Journal of Physics Condensed Matter, 2007. **19**(1).
87. Kumar, P., et al., *Ga-induced superstructures on the Si(1 1 1) 7 × 7 surface.* Applied Surface Science, 2009. **256**(2): p. 480-483.
88. Kumar, P., M. Kumar, and S.M. Shivaprasad, *(7×7) reconstruction as barrier for Schottky-barrier formation at the Ga/Si(111) interface.* Applied Physics Letters, 2010. **97**(12).
89. Kumar, P., et al., *A superstructural 2D-phase diagram for Ga on the Si(111)- 7x7 system.* Solid State Communications, 2011. **151**(23): p. 1758-1762.
90. Otsuka, M. and T. Ichikawa, *New Ga-Induced Superstructures on Si(111) Surfaces.* Japanese Journal of Applied Physics, Part 1: Regular Papers & Short Notes, 1985. **24**(8): p. 1103-1104.
91. Yeom, H.W., K. Yoo, and D.H. Oh, *Electronic structures of Ga-induced incommensurate and commensurate overlayers on the Si(111) surface.* Surface Science, 2011. **605**(1-2): p. 146-152.
92. Cho, K. and E. Kaxiras, *Diffusion of adsorbate atoms on the reconstructed Si(111) surface.* Surface Science, 1998. **396**(1-3): p. L261-L266.
93. Gangopadhyay, S., T. Schmidt, and J. Falta, *Influence of substrate domain boundaries on surface reconstructions of Ga/Si(1 1 1).* Surface Science, 2004. **552**(1-3): p. 63-69.
94. Hibino, H., H. Kageshima, and M. Uwaha, *Instability of steps during Ga deposition on Si(1 1 1).* Surface Science, 2008. **602**(14): p. 2421-2426.
95. Cho, E.S., et al., *High-resolution core-level photoelectron spectroscopy of Mg/Si(100) surfaces.* Surface Science, 2003. **523**(1–2): p. 30-36.
96. Hutchison, P., M.M.R. Evans, and J. Nogami, *Initial stages of Mg growth on the Si(001) surface studied by STM.* Surface Science, 1998. **411**(1-2): p. 99-110.
97. Kawashima, Y., et al., *Surface structures of the Mg/Si(100) system studied by low-energy electron diffraction and Auger electron spectroscopy.* Surface Science, 1994. **319**(1-2): p. 165-171.
98. Kim, J.S., et al., *LEED studies of the adsorption of Mg and Ba on a single domain Si(001)2×1 surface.* Journal of the Korean Physical Society, 1999. **35**(SUPPL. 2): p. S550-S553.
99. Kubo, O., et al., *Mg/Si(100) reconstructions studied by scanning tunneling microscopy.* Japanese Journal of Applied Physics, Part 1: Regular Papers and Short Notes and Review Papers, 2000. **39**(6 B): p. 3740-3743.
100. van Buuren, M.R.J., C.L. Griffiths, and H. van Kempen, *Chemical interactions and Schottky barrier determinations at the Mg/Si(100) interface studied using X-ray photoelectron spectroscopy.* Surface Science, 1994. **314**(2): p. 172-178.
101. Khoo, G.S. and C.K. Ong, *The interactions of metallic and semiconducting adsorbates with Si(100).* Journal of Physics: Condensed Matter, 1994. **6**(40): p. 8141-8148.
102. Shaltaf, R., E. Mete, and Ş. Ellialtioglu, *Mg adsorption on Si(001) surface from first principles.* Physical Review B - Condensed Matter and Materials Physics, 2004. **69**(12): p. 1254171-1254177.

103. Zorin, E.I., et al., *Difference Between the Properties of Sodium- AND Potassium-Doped Silicon.* Soviet Physics Semiconductors, 1972. **6**(2): p. 344-346.
104. Daimon, H. and S. Ino, *Study of the Si(111) 7 × 7 surface structure by alkali- metal adsorption.* Surface Science, 1985. **164**(1): p. 320-326.
105. Ditzinger, U.A., et al., *Photoemission from K/Si(111)7 × 7 and Cs/Si(111)7 × 7.* Surface Science, 1989. **211-212**(C): p. 707-715.
106. Fan, W.C. and A. Ignatiev, *Metal-adsorbate-induced Si(111)-(1×3) reconstruction.* Physical Review B, 1990. **41**(6): p. 3592-3595.
107. Hashizume, T., Y. Hasegawa, and T. Sakurai, *Alkali-metal adsorption on silicon surfaces studied by field ion-scanning tunneling microscopy (FISTM).* Applied Surface Science, 1991. **48–49**(0): p. 119-124.
108. Hashizume, T., et al., *Absolute coverage of K on the Si(111)-3×1-K surface.* Japanese Journal of Applied Physics, Part 2: Letters, 1993. **32**(9 A): p. L1263-L1265.
109. Jeon, D., et al., *Structural and electronic properties of ordered single and multiple layers of Na on the Si (111) surface.* Physical Review Letters, 1992. **69**(9): p. 1419-1422.
110. Magnusson, K.O. and B. Reihl, *Development of the surface electronic structure of K and Cs overlayers on Si(111)7×7.* Physical Review B, 1990. **41**(17): p. 12071-12075.
111. Mizuno, S. and A. Ichimiya, *RHEED study of alkali metals on Si(111) surface.* Applied Surface Science, 1988. **33-34**(C): p. 38-44.
112. Okuda, T., et al., *Surface electronic structure of ordered alkali- and noble metal-overlayers on Si(111).* Applied Surface Science, 1997. **121-122**: p. 89-97.
113. Wan, K.J., X.F. Lin, and J. Nogami, *Comparison of the 3×1 reconstructions of the Si(111) surface induced by Li and Ag.* Physical Review B, 1992. **46**(20): p. 13635-13638.
114. Gurnett, M., et al., *Core-level spectroscopy study of the Li Si (111) -3×1, Na Si (111) -3×1, and K Si (111) -3×1 surfaces.* Physical Review B - Condensed Matter and Materials Physics, 2005. **71**(19): p. 1-9.
115. Sakamoto, K., et al., *Photoemission study of the Si(111)3×1-K surface.* Physical Review B, 1994. **50**(3): p. 1725-1732.
116. Kronik, L. and Y. Shapira, *Surface photovoltage phenomena: theory, experiment, and applications.* Surface Science Reports, 1999. **37**(1-5): p. 1-206.
117. Sommerhalter, C., et al., *High-sensitivity quantitative Kelvin probe microscopy by noncontact ultra-high-vacuum atomic force microscopy.* Applied Physics Letters, 1999. **75**(2): p. 286-288.
118. Himpsel, F.J., G. Hollinger, and R.A. Pollak, *Determination of the Fermi-level pinning position at Si(111) surfaces.* Physical Review B, 1983. **28**(12): p. 7014-7018.
119. Tung, R.T. and L. Kronik, to be published.
120. Morin, F.J. and J.P. Maita, *Electrical Properties of Silicon Containing Arsenic and Boron.* Physical Review, 1954. **96**(1): p. 28-35.
121. Tung, R.T., et al., *Schottky-barrier inhomogeneity at epitaxial NiSi2 interfaces on Si(100).* Physical Review Letters, 1991. **66**(1): p. 72-75.
122. Lide, D.R., *CRC Handbook of Chemistry and Physics*. 90 ed. 2009, CRC Press: Boca Raton.
123. Shannon, J.M., *Increasing the effective height of a Schottky barrier using low-energy ion implantation.* Applied Physics Letters, 1974. **25**(1): p. 75-77.
124. Shannon, J.M., *Reducing the effective height of a Schottky barrier using low-energy ion implantation.* Applied Physics Letters, 1974. **24**(8): p. 369-371.

125. Shannon, J.M., *Control of Schottky barrier height using highly doped surface layers.* Solid State Electronics, 1976. **19**(6): p. 537-543.
126. *Properties of Silicon*. EMIS Datareviews Series, 1988, INSPEC, The Institution of Electrical Engineers: London, New York.
127. Weitering, H.H., et al., *Inhomogeneous Schottky barriers at Ag/Si(111) and Ag/Si(100) interfaces.* Journal of Applied Physics, 1996. **79**(10): p. 7820-7829.
128. Tung, R.T., J.P. Sullivan, and F. Schrey, *On the inhomogeneity of Schottky barriers.* Materials Science and Engineering B, 1992. **14**(3): p. 266-280.
129. Long, W., Y. Li, and R.T. Tung, to be published.
130. Hanbücken, M. and G. Le Lay, *Formation of noble-metal-Si(100) interfaces.* Surface Science, 1986. **168**(1-3): p. 122-132.
131. Le Lay, G., *Physics and electronics of the noble-metal/elemental-semiconductor interface formation: A status report.* Surface Science, 1983. **132**(1-3): p. 169-204.
132. Hiraki, A., *Low temperature reactions at Si/metal interfaces; What is going on at the interfaces?* Surface Science Reports, 1983. **3**(7): p. 357-412.
133. Calandra, C., O. Bisi, and G. Ottaviani, *Electronic properties on silicon-transition metal interface compounds.* Surface Science Reports, 1985. **4**(5-6): p. 271-364.
134. Saiz-Pardo, R., R. Rincón, and F. Flores, *Schottky barrier formation for passivated semiconductor surfaces.* Applied Surface Science, 1996. **92**: p. 362-366.
135. Akiya, M. and H. Nakamura, *Low ohmic contact to silicon with a magnesium/aluminum layered metallization.* Journal Of Applied Physics, 1986. **59**(5): p. 1596-1598.
136. Janega, P.L., et al., *Contact resistivity of some magnesium/silicon and magnesium silicide/silicon structures.* Applied Physics Letters, 1988. **53**(21): p. 2056-2058.
137. Udeshi, D., et al., *Electrical characterization of interface stability between magnesium and selenium-passivated n-type silicon (001).* International Journal Of Electronics, 2005. **92**(12): p. 719-727.
138. Baranek, P., J. Schamps, and I. Noiret, *Ab initio studies of electronic structure, phonon modes, and elastic properties of Mg2Si.* Journal of Physical Chemistry B, 1997. **101**(45): p. 9147-9152.
139. Folland, N.O., *Self-consistent calculations of the energy band structure of Mg2Si.* Physical Review, 1967. **158**(3): p. 764-775.
140. Lee, P.M., *Electronic structure of magnesium silicide and magnesium germanide.* Physical Review, 1964. **135**(4A): p. A1110-A1114.